The computational units of the brain: neuron and column models.

2.1 Introduction.

In the 19^{th} century, innovative staining techniques of the nervous system by pionneers of histology, like Gerlach and Golgi, were used to support the reticular theory of cerebrospinal organization. The brain tissue was considered to be a continuous net of nerve fibers with holistic properties, being an exception to the cell theory. At the end of the 19^{th}, Ramon y Cajal improved Golgi staining techniques and contributed to the opposite theory: the neuron doctrine. The reticular theory was also in contradiction with the localization of function in the brain like the Broca area dedicated to speech production and discovered in 1861. Sherrigton also supported the neuron theory and named synapse the connexion point between two neurons. The neuron is composed of a dendritic arbor on which presynaptic neurons make contact at dendrites, a cell body, also called soma and an axon. If inputs incoming to the cell body are sufficient, a spike is initiatiated at the axon hillock and propagates through the axon. These parts are illustrated on fig 2.1 for a generic neuron but many cell types with their specific morphology are found in the cortex. This all-or-none behaviour was used to design simplified models capturing the computational properties of the neuron, that is the way inputs are combined before deciding whether to spike or not. In a simple example of such artificial neurons, originally proposed by McCullough and Pitts [77], a weighted sum of the inputs is passed through a sigmoid transfer function. Having interesting computational properties, like any boolean function can be implemented by a network of such units, this artificial neural network, sometimes with different transfer functions and additional learning dynamics on the weights, were a key element in the development of

cybernetics and more specifically connectionism. Beside such formal approach, the understanding of the biophysical mechanisms responsible for spike generation and propagation resulted in more realistic models of the neuron dynamics which will be presented in this chapter.

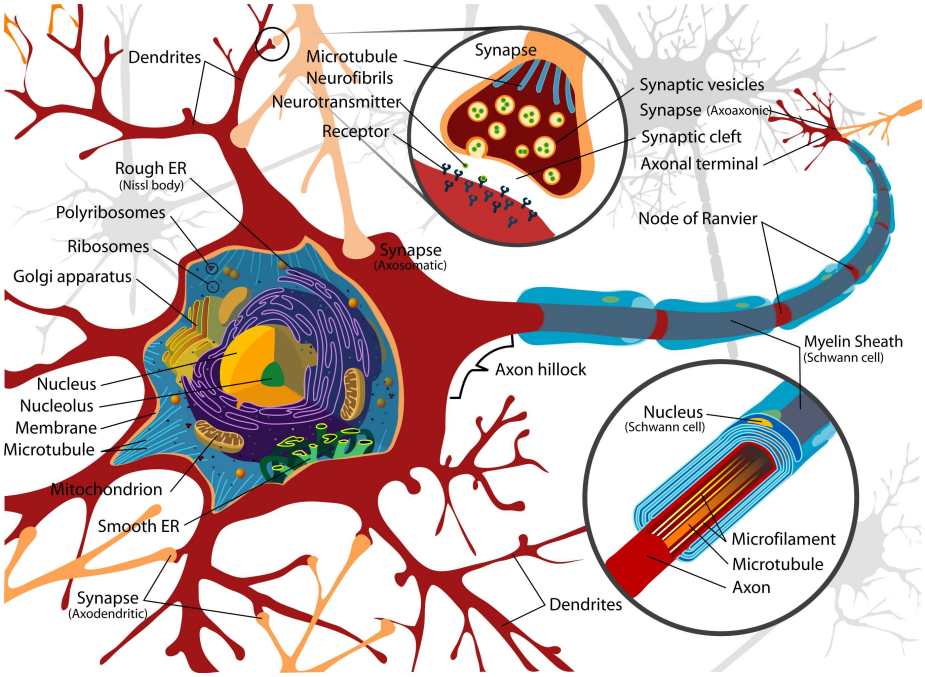

Figure 2.1: **Diagram of a neuron with myalinated axon.** - The dendrites, the soma, the axon and additional structures are indicated (Adapted from http://en.wikipedia.org/wiki/Neuron).

The modular theory of the brain and observations in histology led to the discovery of another set of computational unit at a mesoscale: the cortical columns. Cortical columns have been defined on anatomical ground with minicolumns of $50\mu m$ width containing around a hundred of cells being the result of cell migration during development [78]. The macrocolumn is defined on a functional ground, as described in the introduction, but its anatomical subtrates are estimated of around $300\mu m$ for the visual cortex of the macaque monkey in [79]. A typical macrocolumn contains few thousands of cells and the detailed model of a cortical column of the rat somatosensory cortex in the Blue Brain project contains 10000 neurons of 200 possible types in a space of $500\mu m$ width and $1.5mm$ depth [80]. The column gathers cells coding for the same feature of the inputs so that a feature is reflected in the activity of a population of cells rather than in a single cell spike train. This redundancy in the vertical direction of the cortex makes the code robust to perturbations of the dynamics like synaptic transmission failure or intrinsic fluctuations in cortical dynamics. First

evidences for such columnar organization were found in the somatosensory cortex of the cat by Mounstcastle [81] in the 50s and few years later in Hubel and Wiesel work on the primary visual cortex of the cat [82].

Depending on the animal and the area considered, the neuronal computations can be understood at the single cell level or at the column level, it is thus necessary to analyze models of these computational units with tools from the theory of dynamical systems which will be presented in this chapter. Biologically realistic models of the neuron have several variables (4 in the classical Hodgkin-Huxley model) often following a non-linear evolution equation making their analysis a difficult task. Reduced low dimensional models capture the essential features of the dynamics taking advantage of linearly related variables in the Fitz-Hugh Nagumo model or caricaturating the spike by an instantaneous reset after the membrane crosses a threshold. Models of a cortical column, with their huge state space, can also be reduced by considering the mean field approximation of the network. In this chapter, after presenting the neuron and the cortical column, we give a short introduction to dynamical systems and then apply such methods to models of the computational units of the nervous system.

2.2 Dynamical systems.

A neuron and a column can both exhibit complex dynamics and the theory of dynamical systems is of great use to understand it. The main concepts and some examples are briefly summarized bellow and a full presentation of the bifurcation theory can be found in [83], [84] and [85].

2.2.1 Invariant sets, stability.

A dynamical system consists of the triple T,X,ϕ^t, where T is a time set, X is a state space and ϕ^t is a family of evolution operators parametrized by $t \in T$ and satisfying the following properties: $\phi^0 = id$ and $\phi^{t+s} = \phi^t \circ \phi^s$. Dynamical systems are studied through the orbits they produce and an orbit starting at x_0 is the ordered subset of the state space X, $Or(x_0) = \{x \in X : x = \phi^t x_0$ for all $t \in T$ such that $\phi^t x_0$ is defined$\}$. The phase portrait result from the partitioning of the state space into orbits. Particularly simple orbits consist of fixed points and limit cycles. A point $x_0 \in X$ is a fixed point if $\phi^t x_0 = x_0$ for all $t \in T$. A cycle L_0 is a periodic orbit such that each point $x_0 \in L_0$ satisfies $\phi^{t+T_0} x_0 = \phi^t x_0$ with some $T_0 > 0$, for all $t \in T$. A cycle with no other cycle in the neighborhood is called a limit cycle. Fixed point and limit cycle are two examples of invariant sets that is a subset $S \in X$ such that for each point $x_0 \in S$, $\phi^t x_0 \in S$ for all $t \in T$. Invariant sets more complex than fixed points and cycles are related to chaotic dynamics. An important property of an invariant set is its stability because it determines if nearby orbits will be attracted to this set and then if the invariant will be observable in the dynamics of the system. An invariant set S_0 is Lyapunov stable if for any sufficiently small neighborhood $U \subset S_0$ there exists a neighborhood $V \subset S_0$ such that $\phi^t x \in U$ for all $x \in V$ and all $t > 0$. An

invariant set S_0 is asymptotically stable if there exists a neighborhood $U_0 \subset S_0$ such that $\phi^t \to S_0$ for all $x \in U_0$ as $t \to \infty$. An invariant set is stable if it is both Lyapunov stable and asymptotically stable. A dynamical system can be defined from a system of differential equations, $\dot{x} = f(x)$, where the orbits are the solutions of the system. The fixed point x_0 is stable if the eigenvalues, λ_i, of the Jacobian matrix, $A = f_x(x_0)$, of the system at the fixed point all have negative real part, $Re\lambda_i < 0$. Asymptotic stability of a fixed point x_0 can also be demonstrated if there exists a Lyapunov function for the system near x_0, that is a continuous function defined on a neighborhood of x_0, minimum in x_0 and strictly decreasing on its domain of definition. In some cases, the vector field f defining the dynamical system can be derived from a potential V such that $f = \nabla V$. Fixed points of the system will be critical points of the potential and it will be stable if it is a local minimum.

2.2.2 Bifurcations and normal forms

The phase portrait is a good description of a dynamical system and it can be used to compare different dynamical systems. Thus, two phase portraits are topologically equivalent if there exists a homeomorphism mapping the orbits of one onto the orbits of the other, preserving the direction of time. Fixed points can then be classified into stable node, stable focus, unstable node, unstable focus or unstable saddle (see fig 2.2). If there is no eigenvalue of the Jacobian on the imaginary axis, the fixed point is hyperbolic. When a parameter variation leads to a topologically nonequivalent phase portrait, a bifurcation occurs. The codimension of the bifurcation is the number of independant conditions determining the bifurcation. Informations about these changes are gathered in a bifurcation diagram which represent the phase portrait for various parameter values. An equivalence relation between dynamical systems have to consider a mapping from the parameter space of the first to the parameter space of the second. If we take $\dot{x} = f(x, \alpha)$, $x \in \mathbb{R}^n$, $\alpha \in \mathbb{R}^m$ and $\dot{y} = f(y, \beta)$, $y \in \mathbb{R}^n$, $\beta \in \mathbb{R}^m$, those two dynamical systems are topologically equivalent if there exists a homeomorphism of the parameter space $p : \mathbb{R}^m \to \mathbb{R}^m$, $\beta = p(\alpha)$ and there is a parameter dependent homeomorphism of the phase space h_α: $\mathbb{R}^n \to \mathbb{R}^n$, $y = h_\alpha$, mapping orbits of the first system at parameter values α onto orbits of the second system at parameter values $\beta = p(\alpha)$, preserving the direction of time. The two systems are locally topologically equivalent near the origin if

- there exists a mapping $(x, \alpha) \to (h_\alpha(x), p(\alpha))$ defined in a small neighborhood of $(x, \alpha) = (0, 0)$,
- p is an homeomorphism defined in a small neighborhood of $\alpha = 0$,
- $p(0) = 0$,
- h_α is a parameter dependent homeomorphism defined in a small neighborhood U_α of $x = 0$, with $h_0(0) = 0$, mapping the orbits of the first system in U_α onto the orbits of the second system in $h_\alpha(U_\alpha)$.

(n_+, n_-)	Eigenvalues	Phase portrait	Stability
(0, 2)	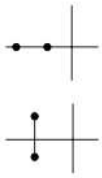	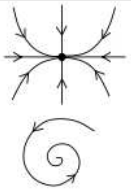 node focus	stable
(1, 1)	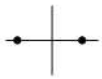	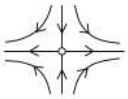 saddle	unstable
(2, 0)	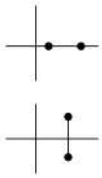	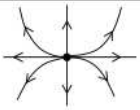 node  focus	unstable

Figure 2.2: **Classification of fixed points for a 2D system.** - Depending on the sign of eigenvalues of the Jacobian, a fixed point can be: stable node, stable focus, unstable node, unstable focus or unstable saddle (Adapted from [83]).

A dynamical system defined by a polynomial with a bifurcation of the origin may be topologically equivalent to a simpler polynomial, that is a polynomial of lower degree or taking the symmetry of the system into account. The simplest of such systems is called a topological normal form for this bifurcation if any generic system [1] with an equilibrium satisfying the same bifurcation condition is locally topologically equivalent near the origin to this system for some values of the coefficient of the polynomial.

2.2.3 Examples of bifurcations.

Fold bifurcation.

The most simple bifurcations are related to the loss of hyperbolicity of a fixed point. The fold (also called saddle-node) bifurcation occurs when the Jacobian matrix at a fixed point has a zero eigenvalue. The simple dynamical system $\dot{x} = x^2 + \alpha$ has a nonhyperbolic equilibrium $x_0 = 0$ with $\lambda = f_x(0,0) = 0$ when $\alpha = 0$. When $\alpha < 0$, there are two equilibria $x_\pm(\alpha) = \pm\sqrt{\alpha}$, with x_+ unstable and x_- stable, and when α crosses zero from negative to positive values, the two equilibria collide and disappear so that there is no equilibrium anymore when $\alpha > 0$ as shown on the bifurcation diagram on fig 2.3. It can be shown that any system with higher order terms is locally topologically equivalent to the previous system. Furthermore, any generic dynamical system having a fold bifurcation of the equilibrium $x_0 = 0$ at $\alpha = 0$ is locally topologically equivalent to $\dot{y} = y^2 + \beta$, which is then a normal form for the fold bifurcation. The conditions for the bifurcation to be generic are the non degeneracy condition, $\frac{1}{2} f_{xx}(0,0)0$, and the transversality condition, $f_\alpha(0,0) \neq 0$.

Hopf bifurcation.

If at some parameter value, eigenvalues are $\pm i\omega$, a Hopf bifurcation occurs with a limit cycle emerging from a fixed point. This can only occur in at least 2 dimensional systems and the topological normal forms for such bifurcation is:

$$\begin{cases} \frac{dx}{dt} &= \beta x - y + sx(x^2 + y^2 - \alpha) \\ \frac{dy}{dt} &= x + \beta y + sy(x^2 + y^2 - \alpha) \end{cases}$$

with $s = \pm 1$ depending on the Lyapunov coefficient of the original system. If $s = -1$, the fixed point becomes repelling at $\alpha = 0$ and the activity follows the branch of the stable periodic orbit, this is the supercritical Hopf bifurcation. If $s = 1$, the Hopf bifurcation is subcritical, unstable periodic orbits colliding with the stable node so that it becomes repelling after the bifurcation and the system jumps to the closest stable set (see fig 2.3).

[1] A generic system satisfies:

- A nondegeneracy condition: at least one coefficient of higher order than linear don't vanish at the bifurcation point.
- A transversality condition: derivative of the real part of the eigenvalue with respect to the bifurcation parameter is non zero a the bifurcation point.

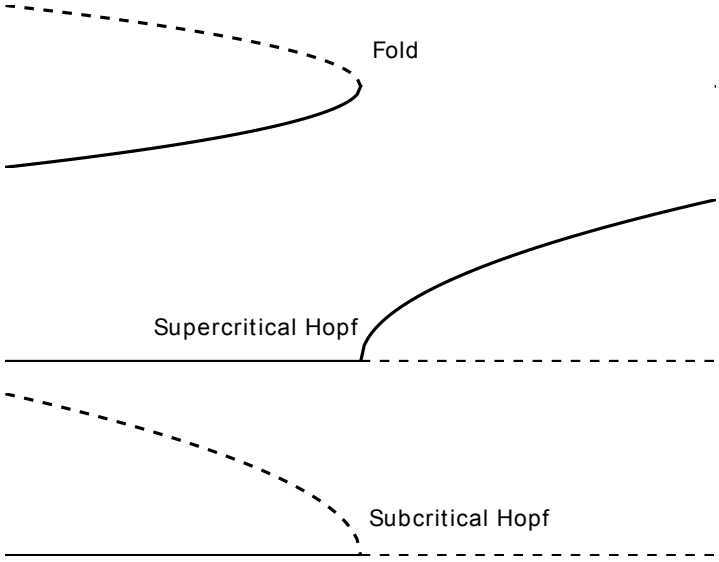

Figure 2.3: **Bifurcation diagrams** - (Up) Fold bifurcation. (Midle) Supercritical Hopf bifurcation. (Down) Subcritical Hopf bifurcation.

Homoclinic orbit.

An orbit starting at x is called homoclinic to the equilibrium x_0 if $\phi^t x \to x_0$ as $t \to \pm\infty$, that is the orbit connects the saddle x_0 to itself. Heteroclinic orbits connect a saddle to another saddle. These phenomena are found for a particular value of the parameter which is an example of global bifurcation.

2.3 Stochastic dynamics.

Often some random behaviour is observed in neuronal data and a noise term is often included in models of neuronal dynamics. Thus to get a good representation of the dynamics, one realization is not enough and it is necessary to consider averages and distributions over an ensemble of realizations of the processes. An introduction to stochastic dynamics and random dynamical systems can be found in [86], [87] and [88].

2.3.1 Stochastic processes.

Definition Given a probability space $(\Omega, \mathcal{F}, P)$, with Ω the set of possible outcomes, $\mathcal{F}$ the set of events and P the probabilities attributed to these events, a stochastic process is a collection of random variables $X_t, t \in T$ defined on $(\Omega, \mathcal{F}, P)$. The process is discrete in time if $T = \mathbf{N}$ and continuous in time if $T = \mathbf{R}^+$. The Markov property characterizes minimal memory processes where the present state is sufficient to get the full distribution over the future, this can be expressed by the following conditional probability distributions:

$$p(x_{k+1}, t_{k+1}; ...; x_n, t_n | x_1, t_1; ...; x_k, t_k) = p(x_{k+1}, t_{k+1}; ...; x_n, t_n | x_k, t_k).$$

A Markovian process checks the Chapman-Kolmogorov equation for transition probabilities:

$$p(x_1, t_1 | x_3, t_3) = \int dx_2 p(x_1, t_1 | x_2, t_2) p(x_2, t_2 | x_3, t_3)$$

.

There are several kinds of stochastic processes:

- Continuous processes where the random variables can take all possible values in their range of definition.
- Jump processes where the random variables can take values on a finite set and jumps from one of this value to another.
- Point processes where event take place at random times.

The definition for the continuity of a stochastic process is given by the Lindeberg condition, for every $\epsilon > 0$:

$$lim_{\Delta t \to 0} \int_{|x-z|>\epsilon} dx p(x, t + \Delta t | z, t) = 0$$

.

The Brownian motion. A simple example of stochastic process checking the Markov property is the Brownian motion [2] $B(t), t \in T$ characterized as follows:

- B(0)=0.
- For all $t_1 < t_2 < ... < t_n$, increments $B(t_2) - B(t_1), ..., B(t_n) - B(t_{n-1})$ are random independent variables.
- For $0 < s < t$, the random variable $B(t) - B(s)$ follows a normal distribution $\mathcal{N}(0, t-s)$
- The transition probabilities of $B(t)$ checks the Lindeberg continuity condition.

The probability distribution of B(t) follows a Gaussian law with mean $\mathbf{E}[B(t)] = 0$ and $\mathbf{E}[B(t)^2] = t$, it is then a solution of the following diffusion equation:

$$\frac{\partial p(x,t)}{\partial t} = \frac{1}{2}\frac{\partial^2 p(x,t)}{\partial x^2}, p(x,0) = \delta(x)$$

having as solution $p(x,t) = \frac{1}{\sqrt{2\pi t}} e^{-\frac{x^2}{2t}}$.

The increments $\Delta B(t_i)$ for a process can be generated by the Box-Mueller algorithm:

- Pick up U and V, random numbers independent and from a uniform law in $[0,1]$.
- Compute $X = \sqrt{-2ln(U)}cos(2\pi V)$ and $Y = \sqrt{-2ln(U)}sin(2\pi V)$.

then X and Y are independent random variables with $\mathcal{N}(0,1)$ as probability density function.

The Poisson process A Poisson process is a counting process, $(N_t)_{t\geq 0}$ a family of random variables indexed by $t \in \mathbf{R}$ and taking values in $\mathbf{N}$ with independent successive increments and the probability distribution of (N_t) only depending on the length of the time intervals. For such a process $(N_t)_{t\geq 0}$ follows a Poisson distribution : $P(N_{t+\tau} - N_t = k) = \frac{e^{\lambda\tau}(\lambda\tau)^k}{k!}$ with λ the rate of the process, times between to events follows an exponential distribution $f(T) = \lambda e^{-\lambda T}$. The average inter events interval is $\mathbf{E}[T] = \frac{1}{\lambda}$ and the variance is $\mathbf{E}[(T - \mathbf{E}[T])^2 = \frac{1}{\lambda^2}$.

Ito processes Ito processes can be written in integral form:

$$x(t) = x(0) + \int_0^t a(x,s)ds + \int_0^t b(x,s)dB(s)$$

[2] It was named after the botanist Robert Brown who observed random trajectories of pollen particles in water and it is sometimes called a Wiener process after the mathematician Norbert Wiener who provided a formalization for it.

or equivalently as a stochastic differential equation [3]:

$$dx(t) = a(x,t)dt + b(x,t)dB(t).$$

Where $a(x,t)$ stands for the deterministic part of the dynamics and $b(x,t)$ for the stochastic part, the noise term is additive if b doesn't depend on x and is multiplicative otherwise. For a multiplicative noise, the integral formula can be interpreted with Ito's definition

$$\int_0^t b(x,s)dB(s) = lim_{n\to\infty} \sum_{i=1}^{n} b(x(t_{i-1}))(B(t_i) - B(t_{i-1}))$$

or with Stratanovich's definition

$$\int_0^t b(x,s)dB(s) = lim_{n\to\infty} \sum_{i=1}^{n} b(\frac{x(t_{i-1}) + x(t_i)}{2}, t_{i-1})(B(t_i) - B(t_{i-1}))$$

but for additive noise the two formulations are equivalent.

2.3.2 Stochastic calculus.

Ito's formula and Forward Kolmogorov equation In stochastic calculus, the chain rule for derivation must be modified because terms of order $(dB(t))^2$ are of same order as dt. The derivative of $y = f(x)$ is then at first order in dt:

$$dy(t) = (\frac{\partial f(x)}{\partial x}a(x,t) + \frac{1}{2}\frac{\partial^2 f(x)}{\partial x^2}b^2(x,t))dt + \frac{\partial f(x)}{\partial x}b(x,t)dB(t).$$

Applying this formula to $\mathbf{E}[f(x)] = \int f(x,t)p(x,t)dx$, with p the probability distribution of x, gives:

$$\frac{d}{dt}\int f(x,t)p(x,t)dx = \int [\frac{\partial f(x)}{\partial x}a(x,t) + \frac{1}{2}\frac{\partial^2 f(x)}{\partial x^2}b^2(x,t)]p(x,t)dx$$

which can be integrated by parts:

$$\frac{d}{dt}\int f(x,t)p(x,t)dx = \int [-\frac{\partial p(x,t)a(x,t)}{\partial x} + \frac{1}{2}\frac{\partial^2 p(x,t)b^2(x,t)}{\partial x^2}]f(x,t)dx.$$

As this is checked for any f, it gives the forward Kolmogorov or Fokker-Planck equation [4]:

$$\frac{dp(x,t)}{dt} = -\frac{\partial p(x,t)a(x,t)}{\partial x} + \frac{1}{2}\frac{\partial^2 p(x,t)b^2(x,t)}{\partial x^2}.$$

It can be generalized to N-dimensional processes so that:

$$d\mathbf{x}(t) = \mathbf{a}(\mathbf{x},t)dt + \mathbf{b}(\mathbf{x},t)d\mathbf{B}(t)$$

[3] called the Langevin equation.

[4] It can also be derived as the Kramers-Moyal expansion of the Chapman-Kolgomogorov equation truncated at order 2, see [87].

have the following Fokker-Planck equation:

$$\frac{\partial p(\mathbf{x},t)}{\partial t} = \sum_{1\leq i\leq N} \frac{\partial a_i((x),t)p(\mathbf{x},t)}{\partial x} + \sum_{1\leq i\leq N}\sum_{1\leq j\leq N} \frac{\partial^2 \mathbf{b}(\mathbf{x},t)\mathbf{b}^T(\mathbf{x},t)p(\mathbf{x},t)}{\partial x_i \partial x_j}.$$

By introducing probability currents, for $1 \leq i \leq N$:

$$J_i = a_i(\mathbf{x},t)p(\mathbf{x},t) - \frac{1}{2}\sum_{1\leq j\leq N} \frac{\partial \mathbf{b}_{ij}(\mathbf{x},t)p(\mathbf{x},t)}{\partial x_j},$$

the Fokker-Planck equation can be written as a conservation law for the probability density:

$$\frac{\partial p(\mathbf{x},t)}{\partial t} + \sum_{1\leq j\leq N} \frac{\partial J_i(\mathbf{x},t)}{\partial x_j} = 0$$

Boundary conditions must be added to be able to solve this equation, it is commonly taken as $lim_{|\mathbf{x}|\to\pm\infty} p(\mathbf{x},t) = 0$ but absorbing or reflecting barriers may be specified.

2.4 Numerical integration and analysis.

We now present some numerical integration schemes for ordinary differential equations with a special focus on explicit methods. In an explicit method x_{n+1} only depends on previous values x_k whereas in implicit methods it alsodepends on itself.

2.4.1 Integration of deterministic systems.

Euler scheme. For a one dimensional dynamical system defined by the following differential equation:

$$\frac{dx(t)}{dt} = f(t, x(t))$$

a trajectory starting at $x(t_0) = x_0$ can be integrated with a time step h by the Euler method, for $n > 0$:

$$x_{n+1} = x_n + hf(t_n, x_n)$$

which is just the approximation obtained by considering the first terms of the Taylor expansion. The higher order approximation is

$$x_{n+1} = x_n + hf(x_n) + h^2(\frac{\partial f}{\partial t}(t_n, x_n) + \frac{\partial f}{\partial x}(t_n, x_n)f(t_n, x_n))$$

so that the error between the numerical solution and the exact solution scales as h^2 thus being of order 1.

Heun scheme The Heun method is another one step integration scheme:

$$x_{n+1} = x_n + \frac{h}{2}(f(t_n, x_n) + f(t_n, u_n + hf(t_n, x_n)))$$

but it is of order 2 so that the error scales as h^3.

Runge Kutta scheme When f is non-linear, errors from the Euler method can be reduced by employing more sophisticated methods like the Runge Kutta methods which includes multiple steps. In the fourth order method, two intermediate points are introduced, so that:

$$x_{n+1} = x_n + \frac{h}{6}\sum_{i=1}^{4} b_i k_i$$

with $b_1 = 1$, $b_2 = 2$, $b_3 = 2$, $b_4 = 1$ and

$$k_1 = f(t_n, y_n)$$

$$k_2 = f(t_n + \frac{h}{2}, x_n + \frac{h}{2}k_1)$$

$$k_3 = f(t_n + \frac{h}{2}, x_n + \frac{h}{2}k_2)$$

$$k_4 = f(t_{n+1}, x_n + \frac{h}{2}k_3)$$

A s stage Runge Kutta method cannot be of order higher than s and this method can be extrapolated to an arbitrary number f stages increasing the accuracy. In the Gill's method, coefficients are a bit modified: $b_1 =, b_2 = 2 - \sqrt{2}, b_3 = 2 + \sqrt{2}, b_4 = 1$ and

$$k_1 = f(t_n, x_n)$$

$$k_2 = f(t_n + \frac{h}{2}, x_n + \frac{h}{2}k_1)$$

$$k_3 = f(t_n + \frac{h}{2}, x_n + \frac{h}{2}(-1 + \sqrt{2})k_1 + h(1 - \frac{\sqrt{2}}{2})k_2)$$

$$k_4 = f(t_n + h, x_n - \frac{h\sqrt{2}}{2}k_1 + (1 + \frac{\sqrt{2}}{2})k_3).$$

These methods can also be improved to implement time step adaptivity.

2.4.2 Integration of stochastic systems

Numerical integration scheme can also be used to integrate stochastic dynamics.

Euler-Maruyama method. For a stochastic differential equations, like with additive noise $dx(t) = f(t,x)h + \sigma(x)dB(t)$, the Euler method can be modified by introducing the stochastic term: $x_{n+1} = y_n + hf(t_n, x_n) + \sigma(x_n)\sqrt{h}(B(t_{n+1}) - B(t_n)$ where $\Delta(B_t) = B(t_{n+1}) - B(t_n)$ are independent and identically distributed random variables of mean 0 and variance 1.

Milstein method Milstein's scheme is as follows:

$$\begin{aligned} x_{n+1} &= y_n + hf(t_n, x_n) + \sigma(x_n)\sqrt{h}(B(t_{n+1}) - B(t_n)) \\ &\quad + h\sigma(x_n)\sigma'(x_n)((B(t_{n+1}) - B(t_n))^2 - 1) \end{aligned}$$

2.4.3 Analysis of dynamical systems.

Spectral analysis. The Fourrier spectrum of the raw stochastic signal is not the best tool for the analysis of a stochastic signal because it will depend on the specific realization of the noise term. The autocorrelation is a better solution for describing properties of the signal. For a signal $y(t)$, the Fourrier transform is $\hat{y}(\omega) = \int_{-\infty}^{\infty} y(t)e^{-i\omega t}dt$ and the autocorrelation is $< y(t+\tau)y^*(t) >= \int\int_{-\infty}^{\infty} P(x_1, t+\tau, x_2, t)dx_1dx_2$. The Wiener-Kintchine theorem then relates the spectral density $S(\omega) =< \hat{y}(\omega)\hat{y} * (0) >$ to the autocorrelation $< y(\tau)y * (0) >$ by $S(\omega) = \int_{-\infty}^{\infty} e^{-i\omega\tau} < y(\tau)y * (0) > d\tau$.

Lyapunov exponent. Dynamical systems are said to be chaotic if their trajectories diverge exponentially. For trajectories separated by δx_0 at initial time, the difference grows as $\delta x(t) = \delta x_0 e^{\lambda t}$ and the growth coefficient λ is a good indicator of chaotic systems when it is positive, it is called the Lyapunov exponent of the system. For multi-dimensional sytems, there are several directions along which coefficients can be contracting ($\lambda < 0$) or expanding ($\lambda > 0$). If there exist an invariant set, like a limit cycle, $\lambda = 0$ along this set. For smooth dynamical systems, chaotic trajectories shows up only when the dimension is at least three. The Lyapunov spectrum (the set of Lyapunov exponents) is usually calculated by following the dynamics of along the Jacobian and then calculating the expansion and contraction rates. For a system

$$\dot{x} = f(x),$$

the equivalent linear system is

$$\dot{u} = Df(x)u.$$

To avoid accumulation of the dynamics of perturbations along the direction corresponding to the maximal Lyapunov exponent, a Gram-Schmidt orthonormalization procedure is usually adopted [89] transforming a set of vectors $(u_1, ..., u_n)$ into a orthonormal basis of $\mathbf{R}^n$ $(v1, ..., v_n)$:

$$w_1 = u_1, v_1 = \frac{w_1}{\|w_1\|}$$

$$w_2 = u_2 - (u_2.v_1)v_1, \frac{w_2}{\|w_2\|}$$
$$\ldots$$
$$w_n = u_n - \sum_{k=1}^{n-1}(u_n.v_k)v_k, \frac{w_n}{\|w_n\|}$$

This orthonormalization procedure is done every T, K times, while equations for x and u are integrated. The i^{th} Lyapunov exponent is computed as $\lambda_i =< ln\|w_i\| >$ with $< . >$ is the average over iterations.

2.5 Neuron

Neurons have a huge diversity in their structure and their dynamic properties. The Neurolex initiative [5] tries to build a common language for their classification following the Petilla classification for GABAergic neurons [90]. We first describe the diversity of cells encountered in the brain and then we show how simple models can account for essential features the dynamics of the membrane potential in spite of the cellular diversity.

2.5.1 Diversity of the cells.

Excitatory and inhibitory cells. The major classification of cells is on their influence to other neurons which is mediated for chemical synapses by neurotransmitters flowing at the synaptic cleft which is the $20nm$ space between axons terminals and dendritic buttons (see fig 2.1). Neuronal interactions depends on the receptor type, AMPA [6] and NMDA [7] synapses are excitatory whereas GABAa and GABAb [8] synapses are usually considered as inhibitory although these synapses have excitatory effect in early developmental stages. Neurons can also interact through electrical synapses, also called, where the signal can be transmitted faster than for chemical and often bidirectionally via physical contact between the two neurons. The effect of such synapses can be depolarizing or hyperpolarizing depending on the presynaptic activity.

Structure. Another way to classify neurons is on their structure. The most common and biggest neuron in the cortex is the excitatory pyramidal cell which has a triangular soma, a dense dendritic tree with apical and basal parts and a long myelinated axon. Another class of excitatory cells are spiny stellate cells having a symmetric star shape with localized axon. The majority of inhibitory interneurons in layer IV are basket cells. Another class of GABAergic inhibitory interneurons, the chandelier cell, is named after the shape of its axon terminals and the Purkinje cell, also GABAergic but located in the cerebellar cortex, is famous for its beautiful planar dendritic arbor.

[5] Available at http://www.neurolex.org.
[6] AMPA stands for α-amino-3-hydroxy-5-methylisoazol-4-propionate
[7] NMDA stands for N-methyl-D-aspartic acid
[8] GABA stands for gamma-aminobutyric acid.

Channels. The membrane of a neuron includes many voltage gated channels letting ions flow inside or outside the cell depending on the membrane voltage. These channels can also be used to classify neurons. Potassium and sodium channels are present for all neuron types and explain spike generation in the Hodgkin-Huxley model. Other channels are involved in more specific processes like the T-type voltage-gated calcium channel, responsible for the tonic bursting of thalamic cells.

Firing pattern. Neurons can also be classified based on their firing properties in response to a step of input current [91]. Inhibitory interneurons are often fast spiking cells with constant and short interspike interval (ISI). Excitatory cells have different patterns like non-adapting regular spiking with constant ISI but longer than for fast spiking cells. For adapting regular spiking cells, ISI decreases during the response. Intrinsic bursting cells fire with few spikes very close together at the response onset. The Petilla classification includes more complex firing patterns like stuttering, irregular or accelerating. For some neurons, the study of the after potential hyperpolarization can also be helpful for classification.

2.5.2 Dynamic processes.

Models of the dynamics of the membrane potential should include a spike generation mechanism and also describe the synaptic interaction.

Spike generation. The generation of spikes is attributed to two ionic concentrations: K^+ and Na^+. At rest, potassium ions are in excess outside the cell and sodium ions are in excess inside the cell. When the concentrations of these ions inside and outside the cell are balanced to reach equilibrium, the corresponding difference of potential between the inside and the outside is given by the Nernst potential defined as

$$E_{Nernst} = \frac{RT}{z\mathcal{F}} ln \frac{c_{out}}{c_{in}},$$

with

$$R = 6.02.10^{23} mol^{-1}$$

the Avogadro constant ,

$$\mathcal{F} = 9.6510^{-4} C.mol^{-1}$$

the Faraday constant, T the temperature, z the number of charges carried by the ion and c_{in},c_{out} the ion concentrations inside and outside the cell. When the membrane potential deviates from this value, a ionic current is generated proportional to the deviation $(V - E_{Nernst})$ (with $E_K = -77mV$, $E_{Na} = 50mV$). Moreover, the coefficient of proportionality of this current is constant for a passive channel like the leak current $I_L = g_L(V - E_L)$ (with $E_L = -65mV$) but

it depends on the voltage for active channels like the Na and K channels. Each ion flux is conditioned on the opening or closing of active gates. Each gate can be open or closed with transition probability from open to close $\alpha(V)$ and from closed to open $\beta(V)$. The fraction of open channels follows the dynamics:

$$\frac{dm}{dt} = \alpha(V)(1-m) - \beta(V)m$$

or equivalently:

$$\frac{dm}{dt} = \frac{(m_\infty - m)}{\tau(V)}$$

with $m_\infty = \frac{\alpha(V)}{\alpha(V)+\beta(V)}$ and $\tau(V) = \frac{1}{\alpha(V)+\beta(V)}$. In the Hodgkin-Huxley model, 3 channel variables are considered: one for the fraction of activation of the potassium gate n, one for the fraction of activation of the sodium gate m and one for the fraction of inactivation of the sodium gate $1-h$. The current corresponding to these ionic transports are

$$I_K = g_{\bar{K}} n^4 (V - E_K)$$

and

$$I_N a = g_{\bar{N}a} h m^3 (V - E_{Na})$$

with $\bar{g}_K$ and $\bar{g}_{Na}$ the maximal conductances. When the cell is slightly depolarized Na channels open and flow inside the cell, while V is increasing until the driving current proportional to $(V - E_{Na})$ becomes small and Na gets inactivated. Then K currents activate and the potassium driving force $(V - E_K)$ is strong so that the membrane potential decreases and return to its resting value.

Synapse dynamics. An action potential propagates along the axon and when it reaches the synaptic terminals, neurotransmitters are released in the synaptic cleft and postsynaptic events are triggered in the postsynaptic neuron. The corresponding current is

$$I_{syn} = g_{syn}(t)(V(t) - E_{syn})$$

with the synaptic conductances $g_{syn}(t) = \bar{g}_{syn} s(t)$ generated from the incoming spikes by the following dynamics:

$$\tau_{syn} \frac{ds}{dt} = -s + \tau_{syn} \sum_k \delta(t - t_k)$$

where k runs over all presynaptic spikes and the Dirac impulse defined as $\delta(x) = 0$ for $x = 0$ and 0 elsewhere. The solution for s is a sum of exponential $s(t) = \sum_k e^{-\frac{(t-t_k)}{\tau_{syn}}}$. When the dynamics for s is of second order:

$$\frac{d^2 s}{dt^2} + \frac{2}{\tau_{syn}} \frac{ds}{dt} + \frac{1}{\tau_{syn}^2} s = \frac{1}{\tau_{syn}^2} \sum_k \delta(t - t_k),$$

the solution is a sum of α-functions:

$$s(t) = \sum_k \frac{t}{\tau_{syn}^2} e^{-\frac{(t-t_k)}{\tau_{syn}}}.$$

The synaptic reversal potential is $E_E = 0mv$ for excitatory synapses and $E_I = -80mV$ for inhibitory synapses. For electrical synapses, the synaptic current are: $I_{syn} = \bar{g}_{syn}(V_{post} - V_{pre})$. Slow dynamics, like depression, facilitation or spike timing dependent plasticity can also be included in a synapse [92] [93].

Membrane equation. The membrane of the neuron can be seen as a capacitive medium and an equivalent cable equation can be written to describe the propagation of an action potential along the passive parts of the cell the Rall model:

$$C\frac{dV}{dt} = -V + \frac{d^2V}{dx^2}.$$

Active currents responsible for the generation of the action potential are included in a space clamped version of the model with the equivalent circuit drawn on fig . Applying the Kirchoff law in this circuit gives the Hodgkin-Huxley equation:

$$C\frac{dV}{dt} = -I_m - I_E - I_I$$

with $I_m = \sum_i g_i(V - E_i)$ $(i = K, Na, L)$ the intrinsic currents and $I_{E,I} = g_{E,I}(V - E_{E,I})$ the synaptic currents.

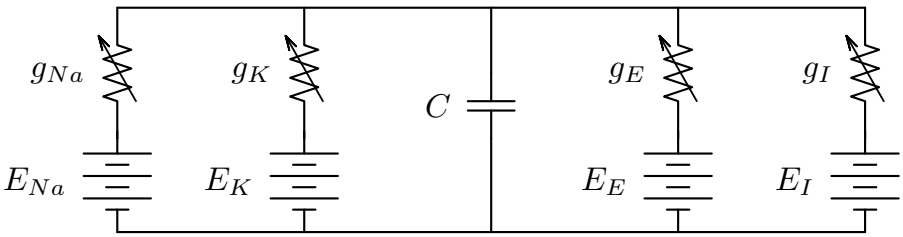

Figure 2.4: **Equivalent circuit for the Hodgkin-Huxley neuron.** - Voltage-gated sodium and potassium channels (g_{Na}, g_K) and synaptic channels and synaptic channels (g_E, g_I). The capacity C scales the membrane time constant.

2.6 FitzHugh Nagumo model of cell excitability

2.6.1 Derivation of the model

The full Hodgkin-Huxley (HH) system of equations describing the dynamics of the membrane potential of a neuron is difficult to study and in th 60's, it was difficult to simulate. Fitz-Hugh and Nagumo thus used the simplified system

which shares many properties with the full system and make a geometric analysis feasible. The system is composed of two variables at different time scales tuned by the parameter ϵ, the limit $\epsilon \to 0$ making it a slow-fast system.

Starting from the HH equations, two approximations reduce the 4-dimensional system to a 2-dimensional system. The full HH system takes sodium, potassium and leak currents into account:

$$\begin{aligned}
C_m \frac{dV}{dt} &= I(t) - \overline{g}_l(V - E_l) - \overline{g}_K n^4 (V - E_K) - \overline{g}_{Na} m^3 h (V - V_{Na}) \\
\tau_n(V) \frac{dn}{dt} &= n_\infty(V) - n(t) \\
\tau_h(V) \frac{dh}{dt} &= h_\infty(V) - h(t) \\
\tau_m(V) \frac{dm}{dt} &= m_\infty(V) - m(t)
\end{aligned}$$

with

$$\begin{aligned}
\tau_{(n,h,m)} &= \frac{1}{\alpha_{(n,h,m)} + \beta_{(n,h,m)}}, \\
(n_\infty, h_\infty, m_\infty) &= \frac{\alpha_{(n,h,m)}}{\alpha_{(n,h,m)} + \beta_{(n,h,m)}}, \\
\alpha_n &= \frac{.01(V+55)}{1 - e^{-.1(V+55)}}, \\
\beta_n &= .125 e^{-.0125(V+65)} \\
\alpha_h &= 0.07 e^{-.05(V+65)}, \\
\beta_h &= \frac{1}{1 + e^{-.1(V+35)}}, \\
\alpha_m &= \frac{.1(V+40)}{1 - e^{-.1(V+40)}}, \\
\beta_m &= 4 e^{.0556(V+65)}.
\end{aligned}$$

Simulations of these dynamics suggest that some approximations leading to a simpler formulation. The dynamics in the middle panel of figure 2.5 shows that variations of m are quasi-instantenous, so that $m(t) \approx m_\infty(V)$ and the model can be reduced to become 3-dimensional. As seen in the bottom panel of figure 2.5 and in the left panel of figure 2.6, n and h are close to the relation $1.1n(t)+h(t) \approx 0.89$, that brings the model to a 2-dimensional simplified system:

$$\begin{aligned}
C_m \frac{dV}{dt} &= I(t) - \overline{g}_l(V - E_l) - \overline{g}_K n^4 (V - E_K) \\
&\quad - \overline{g}_{Na} \overline{m}_\infty(V)(0.89 - 1.1n)(V - V_{Na}) \\
\tau_n(V) \frac{dn}{dt} &= n_\infty(V) - n(t)
\end{aligned}$$

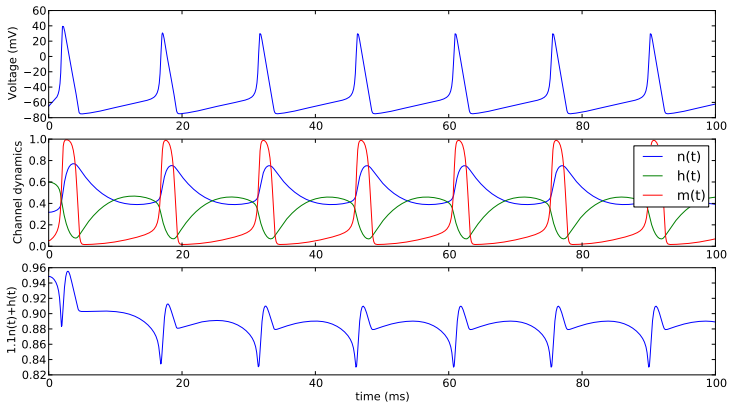

Figure 2.5: Simulation of the Hodgkin-Huxley model. (Up) Dynamics of the membrane potential. (Middle) Dynamics of the activation and inactivation variables of the ionic channels. (Down) 1.1 n(t)+h(t).

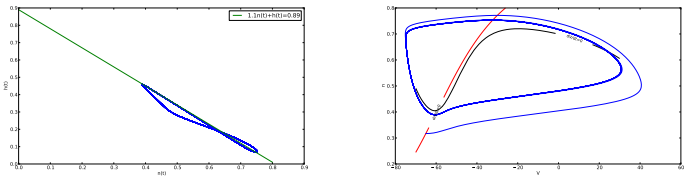

Figure 2.6: (Left) (n,h) dynamics and the line 1.1 n+h=0.89 (Right) (V,n) dynamics and nullclines of the reduced 2D system

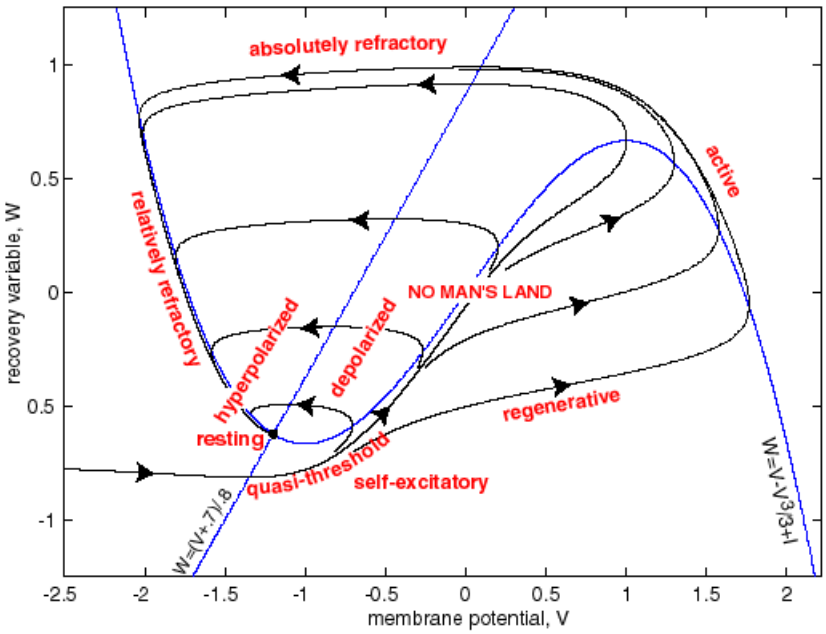

Figure 2.7: Phase portrait of Fitzhugh Nagumo system (Adapted from the Scholarpedia.org article on the FitzHugh-Nagumo model

In the right panel of figure 2.6, the V-nullcline has a N-shape so that it can be approximated by a cubic function and the slow nullcline can be approximated by a straight line leading to the FitzHugh-Nagumo equations:

$$\left\{ \begin{array}{rcl} \epsilon \frac{dx}{dt} & = & x - \frac{x^3}{3} + y \\ \frac{dy}{dt} & = & -(x - a + by) \end{array} \right.$$

with $\epsilon > 0$.

2.6.2 Fixed points, saddle-node bifurcation, cusp

Nullclines are

$$\left\{ \begin{array}{rcl} y & = & -x + \frac{x^3}{3} \\ y & = & \frac{a-x}{b} \end{array} \right.$$

Fixed points are at the intersection of these lines and are the roots of $\frac{x^3}{3} + (-1 + \frac{1}{b})x - \frac{a}{b}$ which is of the form $x^3 + px + q = 0$ and can be solved using Cardan's method.

Here $p = 3(-1 + \frac{1}{b})$ and $q = -3\frac{a}{b}$, the discriminant is $\Delta = q^2 + \frac{4}{27}p^3$:

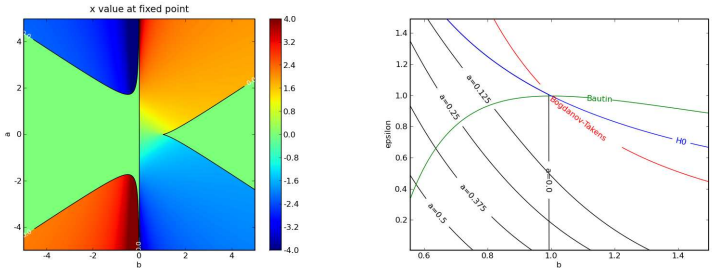

Figure 2.8: (Left) x_0 plotted in color depending on a and b. There are three fixed points in the green areas, the black line is the curve of fold bifurcations and a cusp bifurcation occur at $(1, 0)$.(Right) The red area is where $det(J_{|x_0}) > 0$

- If $\Delta \geq 0$, there is only one real root to the system :

$$x_0 = \sqrt[3]{\frac{-q + \sqrt{\Delta}}{2}} + \sqrt[3]{\frac{-q - \sqrt{\Delta}}{2}}$$

- if $\Delta < 0$ it has 3 solutions($k \in 0, 1, 2$):

$$x_k = 2\sqrt{\frac{-p}{3}} \cos(\frac{1}{3} \arccos(\frac{-q}{2}\sqrt{\frac{27}{-p^3}}) + \frac{2k\pi}{3})$$

A **fold bifurcation** occurs when $det(J_{|x_0}) = \frac{-b(1-x_0^2)+1}{\epsilon} = 0$, it is the line separating the 3 fixed points zone from the one fixed point zone as shown on fig 2.8. When $a = 0$, fixed points are roots of $-\frac{x^3}{3} + (1 - b)x + a$ which is the normal form of a **cusp bifurcation** at $(b = 1, a = 0)$.

2.6.3 Stability of the fixed point when $\Delta > 0$, Hopf and generalized Hopf

Stability matrix near equilibrium x_0:

$$J_{|x_0} = \begin{pmatrix} \frac{1-x_0^2}{\epsilon} & \frac{1}{\epsilon} \\ -1 & -b \end{pmatrix}$$

thus $det(J_{|x_0}) = \frac{-b(1-x_0^2)+1}{\epsilon}$ and $tr(J_{|x_0}) = \frac{1-x_0^2}{\epsilon} - b$.
The characteristic equation is given by:

$$\begin{aligned} P(\lambda) &= \lambda^2 - tr(J_{|x_0})\lambda + det(J_{|x_0}) \\ &= \lambda^2 - (-b + \frac{(1 - x_0^2)}{\epsilon})\lambda + \frac{-b(1 - x_0^2) + 1}{\epsilon} \end{aligned}$$

$$\Delta' = tr(J_{|x_0})^2 - 4det(J_{|x_0}) = (-b + \frac{(1-x_0^2)}{\epsilon})^2 - 4\frac{-b(1-x_0^2)+1}{\epsilon}$$

and eigenvalues of $J_{|x_0}$ are

$$\lambda_\pm = \frac{tr(J_{|x_0}) \pm \sqrt{tr(J_{|x_0})^2 - 4det(J_{|x_0})}}{2}$$

thus damping is $\mu = \frac{1}{2}tr(J_{|x_0})$ and frequency modulation is $\omega = \frac{1}{2}\sqrt{tr(J_{|x_0})^2 - 4det(J_{|x_0})}$.
Andronov-Hopf bifurcation occurs when:

$$\begin{aligned} tr(J_{|x_0}) &= (-b + \frac{(1-x_0^2)}{\epsilon}) = 0 \\ det(J_{|x_0}) &= \frac{-b(1-x_0^2)+1}{\epsilon} > 0 \end{aligned}$$

at the bifurcation point $b = \frac{(1-x_0^2)}{\epsilon}$ and $\lambda_\pm = \pm i\sqrt{-b^2 + \frac{1}{\epsilon}} = \pm i\omega_0$.

To get the normal form, we change coordinates introducing the following vectors:

$q = \begin{pmatrix} -(b+\lambda_+) \\ 1 \end{pmatrix}$ is eigenvector of $J_{|x_0}$ related to λ_+.

$p = \begin{pmatrix} \epsilon(b+\lambda_-) \\ 1 \end{pmatrix}$ is eigenvector of ${}^T J_{|x_0}$ related to λ_-.

The scalar product is $< p, q >= (\hat{p_1}q_1 + \hat{p_2}q_2) = 2\epsilon b(-b + i\omega)$.

We then normalize p taking: $p \to \frac{p}{<p,q>}$ so that: $p = \begin{pmatrix} -\frac{i}{2\omega} \\ 1 - i\frac{b}{\omega} \end{pmatrix}$

We now make the change of coordinates $z =< p, x >$ and with F the non-linear part of the system, the complex variable z is solution of the system:

$$\dot{z} = \lambda_+ z + < p, F(zq, \overline{zq}) >= \lambda z + \sum_{1 \le k+l \le 3} \frac{g_{kl}}{k!l!} z^k \overline{z}$$

$$g(z, \overline{z}) =< p, F(X_0 + zq + \overline{zq}) >$$

$$g(z, \overline{z}) = \frac{i}{2\epsilon\omega}(-\frac{(zq)^3}{3} - \frac{(\overline{zq})^3}{3} - zq(\overline{zq})^2 - (zq)^2\overline{zq} - x_0(zq)^2\overline{zq} - x_0 zq(\overline{zq})^2 - 2x_0 zq\overline{zq})$$

Coefficients of the Taylor expansion are $g_{20} = \frac{-ix_0}{\omega\epsilon^2}((2b^2\epsilon - 1) + 2\epsilon\omega b)$, $g_{11} = \frac{-ix_0}{\omega\epsilon^2}$, $g_{21} = \frac{-\omega + ib}{\omega\epsilon^2}$.

It can be shown that z can be changed to a variable w which after rescaling of the time is solution of the normal form:

$$\dot{w} = (\beta + i)w + l_1 w|w|^2$$

with $\beta = \frac{\mu}{\omega}$ and $l_1 = Re\frac{1}{2\omega}(ig_{20}g_{11} - 2i|g_{11}| - \frac{i}{3}|g_{02}| + \omega g_{21})$ and more simply at the bifurcation :

$$l_1 = \frac{1}{2\omega^2} Re(ig_{20}g_{11} + \omega g_{21})$$

.

$$l_1 = \frac{-\epsilon\omega^2 + 2x_0^2 b}{\epsilon^3 \omega}$$

The sign of the first Lyapunov coefficient characterizes the Hopf bifurcation:

- If $l_1 < 0$, a stable limit cycle emerges at the bifurcation point, it is a **supercritical bifurcation**.
- If $l_1 > 0$, an unstable limit cycle emerges at the bifurcation point, it is a **subcritical bifurcation**.
- **Bautin bifurcation** occurs when $l1 = 0$, that is when $\epsilon = \frac{2b-1}{b^2}$.

There are two possible normal forms for the Bautin bifurcation depending on the sign of the higher order terms (second Lyapunov coefficient l_2):

$$\dot{z} = (\beta_1 + i)z + \beta_2 z|z|^2 \pm z|z|^4$$

with coefficients $\beta_1 = \frac{Re(\lambda)}{Im(\lambda)}$ and $\beta_2 = \sqrt{l_2} l_1$. A polar coordinate transformation, $z = re^{i\phi}$, of the - normal form gives:

$$\left\{ \begin{array}{rcl} \dot{\rho} & = & \rho(\beta_1 + \beta_2\rho^2 - \rho^4), \\ \dot{\phi} & = & 1. \end{array} \right.$$

The only equilibrium is $\rho = 0$ and $\beta_1 + \beta_2\rho^2 - \rho^4 = 0$ may have zero, two or only one solution at the fold of cycles point. There are thus two branches starting from the Bautin point:

- A line H of Hopf bifrcations, $beta_1 = 0$, supercritical for $\beta_2 < 0$ and subcritical for $\beta_2 > 0$.
- A curve $\beta^2 + 4\beta_1 = 0$ with $\beta_2 > 0$, where two limit cycles collide.

Bogdanov-Takens bifurcation occurs when:

$$\left\{ \begin{array}{rcl} tr(J_{|x_0}) & = & (-b + \frac{(1-x_0^2)}{\epsilon}) = 0 \\ det(J_{|x_0}) & = & \frac{-b(1-x_0^2)+1}{\epsilon} = 0 \end{array} \right.$$

that is when $\epsilon = \frac{1}{b^2}$. The normal forms for this bifurcation are:

$$\left\{ \begin{array}{rcl} \dot{\eta_1} & = & \eta_2, \\ \dot{\eta_2} & = & \beta_1 + \beta_2\eta_1 + \eta_1^2 \pm \eta_1\eta_2. \end{array} \right.$$

Moreover, there are three branches passing through the Bogdanov-Takens bifurcation point:

- The line, $\beta_1 = 0$, of Hopf bifurcations.

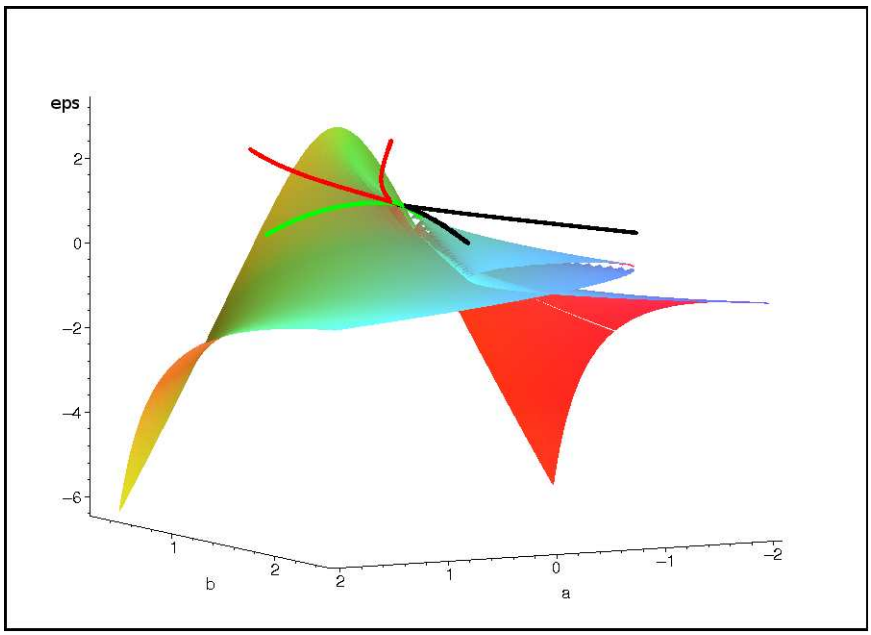

Figure 2.9: (Colored surface) Hopf bifurcation curves ($tr(J_{|x_0}) = 0$) for various values values of a. (Black curve) Fold bifurcation for $\epsilon = 1$, it is the invariant along the ϵ axis. (Red line) Bogdanov-Takens bifurcation curve ($det(J_{|x_0}) = 0$). (Green line) Bautin bifurcation curve ($l_1 = 0$).

- The parabola, $4\beta_1 - \beta_2^2 = 0$, of fold bifurcations.
- The half parabola , $\beta_1 = -\frac{6}{25}\beta_2^2$, of saddle homoclinic bifurcation.

The different types of bifurcation (fold, Hopf, Bautin and Bogdanov-Takens) are represented on the 3D parameter space in fig 2.9. The vertical line of cusp bifurcations,$(b = 1, a = 0)$, and curves for Bautin and Bogdanov-Takens bifurcations intersect at $(b = 1, a = 0, \epsilon = 1)$, this singular situation indicates that this point is a codimension three bifurcation point. It is the organizing center for the dynamics and any behavior of the system is accessible in its neighborhood (except those associated with the slow-fast limit $\epsilon \to 0$).

A normal form for the codimenson three bifurcation point was found along the cusp line in [94]. The system is shown to be topologically equivalent to the following system:

$$\begin{cases} \dot{x_1} &= y_1 - \frac{x_1^3}{3}, \\ \dot{y_1} &= -\frac{x_1^3}{3}. \end{cases}$$

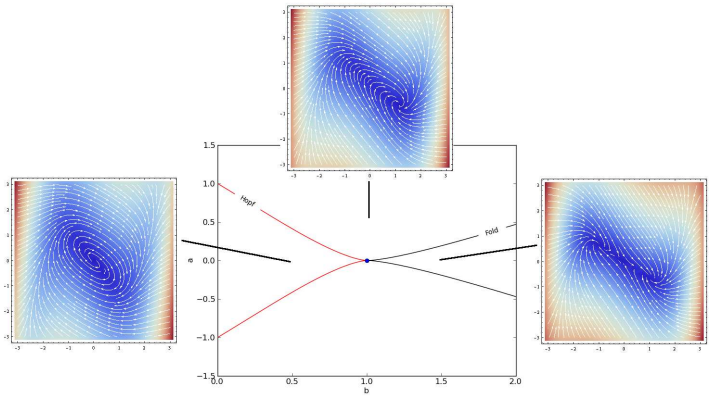

Figure 2.10: Fold and Hopf bifurcation curves starting from the organizing center $\epsilon = 1$ and examples of vector fields.

2.6.4 Dynamics at the organizing center with noisy input.

Bifurcation diagram near $(a = 0, b = 1, \epsilon = 1)$ with example of vector fields (one fixed point, two fixed points and limit cycle) are illustrated on fig 2.10. There is a limit cycle inside the Hopf region, there are 3 fixed points, two of which are stable, inside the fold region and there is a single fixed point elsewhere.

By adding a random component being a Brownian motion, the dynamics writes:

$$\left\{ \begin{array}{rcl} \epsilon dx & = & (x - \frac{x^3}{3} + y)dt + \sigma\sqrt{dt}dB_t \\ dy & = & -(x - a + by)dt \end{array} \right.$$

The associated Fokker Planck equation is:

$$\frac{\partial P}{\partial t} = -\frac{\partial}{\partial x}[(x - \frac{x^3}{3} + y)P] - \frac{\partial}{\partial x}[(x - a + by)P] + \frac{\sigma}{2}\frac{\partial^2 P}{\partial x^2}$$

In fig 2.11, the dynamics of x is shown for three different noise variance but with the same realization of the random process integrated with a stochastic Heun scheme. Although different noise variances are used, the irregularities are similar within the 3 traces.

The power spetrum density is then computed for different values of σ and the frequency F_0 at which this power is maximum is reported on fig 2.12 and 2.13. When the random process is initialized by different seeds, F_0 increases smoothly with σ whereas it increases by jumping from one plateau to another when the same noise realization is used.

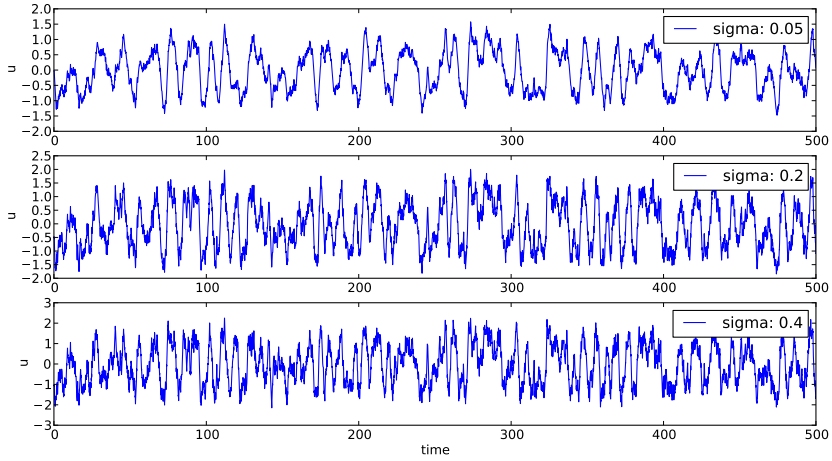

Figure 2.11: Examples of traces for various sigma.

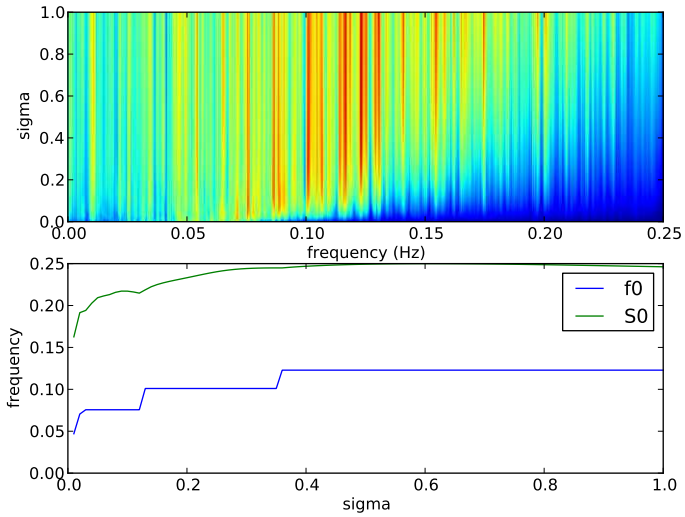

Figure 2.12: (Up) Spectrum for big values of the noise variance. (Down) Dominant frequency F_0 of the spectrum and energy S0 at this frequency. Noise realization are the same for all tested σ.

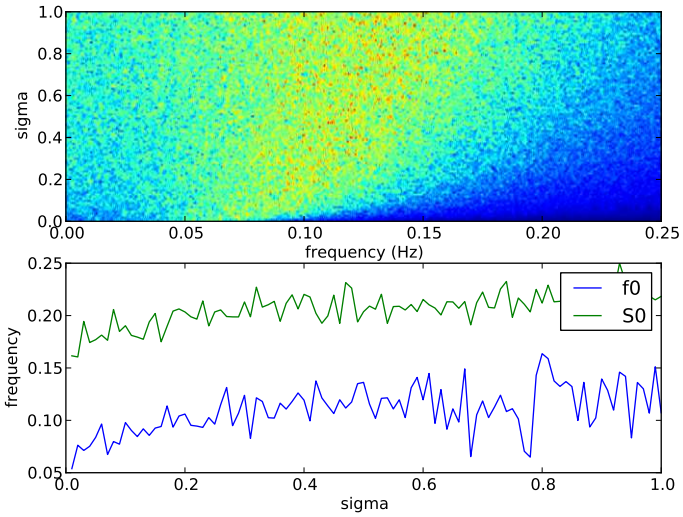

Figure 2.13: (Up) Spectrum for big values of the noise variance. (Down) Dominant frequency F_0 of the spectrum and energy S0 at this frequency. Noise realisation are different for all tested σ.

Lyapunov exponents calculated for different values of σ do not show chaotic dynamics as it stays negative on fig 2.14. In a wavelet analysis, bumps of high power are visible in two frequency bands. The low frequency component could result from noise induced switching between two stable fixed points inside the fold region and the high frequency component could be related to the limit cycle inside the Hopf region.

2.7 Hybrid dynamical systems.

In the Fitz Hugh Nagumo approximation of the membrane potential, the 2 dimensions dynamical system was smooth but the dynamics can also be reduced with a combination of smooth and discontinuous dynamics, with an instantaneous reset from the spike threshold to the resting potential. Such systems combining continuous and discontinuous dynamics are referred as hybrib systems [95].

2.7.1 Integrate and fire neuron models.

Leaky integrate and fire neuron (LIF): constant input. The simplest neuron model after the simple Poisson process consist of the membrane equation with a leak current and external input, spikes are generated by a discontinuity so that the membrane potential is reset to V_r when the voltage crosses a threshold

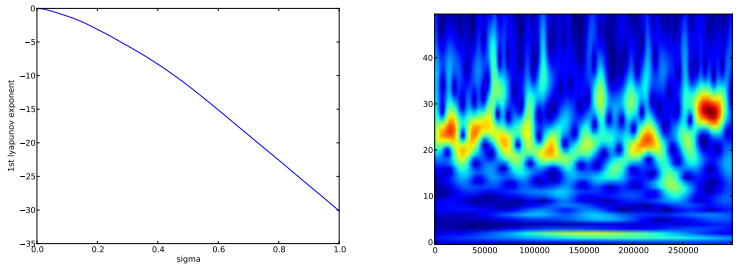

Figure 2.14: (Left) Lyapunov exponents depending on sigma. (Right) Time-frequency analysis of the signal with time steps on the horizontal axis and frequency in Hertz on the vertical axis.

value V_{th}. The dynamics then follows:

$$C\frac{dV}{dt} = -g_L(V - E_L) + I_{ext}$$

$$\text{If } V(t^-) > V_T \text{ then } V(t^+) = V_r.$$

In the case of constant external input I_0 applied by an electrode to an isolated neuron with no synaptic inputs, there is a threshold current $I_T = g_L(V_T - E_L)$ so that if $I < I_T$, the stable fixed point solution is the subthreshold potential $V_\infty = E_L + \frac{I_0}{g_L}$ and if $I > I_{th}$, the neuron spikes regularly. The time dependent solution of the equation is $V(t) = V_\infty + Ae^{-\frac{t}{\tau}}$ with $A = V(0) - V_\infty$ and the time constant, $\tau = \frac{C}{g_L}$. Considering the potential initially at its reset value, $V(0) = V_r$, the threshold is reached at time T so that $V_{th} = V_\infty + (V_r - V_\infty)e^{-\frac{T}{\tau}}$ and thus the stationary interspikes interval of the neuron is

$$T = \tau ln\frac{V_T - V_\infty}{V_r - V_\infty}$$

.

2.7.2 Diffusion approximation of Poissonian input.

In the Stein model [96], the free membrane potential (without considering the threshold for spikes) follows the stochastic differential equation (considering the normalized voltage $V \to g_L(V - E_L)$:

$$dV(t) = -V(t)dt + s_E dN_E(t) + s_I dN_I(t)$$

where N_E,N_I are Poisson processes of rates λ_E, λ_I simulating incoming spike trains and $s_E > 0$,$s_I < 0$ the amplitude of excitatory and inhibitory synaptic events. The diffusion approximation consist in taking simultaneously the limits of small amplitude of synaptic events and large rates of the Poisson processes,

it was shown in [97] that this model converges in law to the following Orstein-Uhlenbeck process:

$$dV(t) = (-V(t) + \mu)dt + \sigma dB(t)$$

with

$$\mu(t, v_0) = v_0 e^{-t} + (s_E \lambda_E + s_I \lambda_I)(1 - e^{-t})$$

and

$$\sigma^2(t, v_0) = \frac{s_E^2 \lambda_E + s_I^2 \lambda_I}{2}(1 - e^{-2t})$$

the drift and diffusion coefficients. The stationary density for the membrane potential is the following Gaussian probability distribution:

$$p(V, t|v_0, 0) = \frac{1}{\sqrt{2\pi\sigma^2(t, v_0)}} e^{-\frac{(V-\mu(t,v_0)^2}{2\sigma^2(t,v_0)}}.$$

2.7.3 Fokker-Planck equation.

We consider the LIF model:

$$C\frac{dV}{dt} = -g_L(V - E_L) + I_{ext}$$

$$\text{If } V(t^-) > V_{th} \text{ then } V(t^+) = V_r$$

with a refractory period τ_r during which V is clamped to the reset value. The Fokker-Planck equation for the probability distribution of the membrane potential is:

$$\frac{\partial P(V,t)}{\partial t} = \frac{\partial (g_L(V - E_L) - \mu)P(v,t)}{\partial v} + \sigma^2 \frac{\partial^2 P(V,t)}{\partial V^2} + r(t)\delta(V - V_r)$$

with μ and σ taken from the diffusion approximation and $\delta(x) = \begin{cases} 1 & \text{if } x = 0 \\ 0 & \text{else} \end{cases}$.

It can be written in the form of a conservation law:

$$\frac{\partial P(V,t)}{\partial t} = -\frac{\partial J(V,t)}{\partial V}$$

with the probability current

$$J(v,t) = (-g_L(V - E_L) + \mu)P(v,t) + \sigma^2 \frac{\partial P(V,t)}{\partial V} + r(t)H(V - V_r)$$

with H the Heaviside function. Boundary conditions on the lower part are $lim_{V\to-\infty} P(V,t) = 0$ and $lim_{V\to-\infty} VP(V,t) = 0$ so that $\int_{-\infty}^{V_T} P(V,t)dV$ is finite. At the threshold, the condition is absorbing $P(V_T, t) = 0$ and the probability current through threshold is the firing rate $r(t)$ so that

$$\frac{\partial P(V_T,t)}{\partial V} = -\frac{r(t)}{\sigma^2}.$$

Taking neurons in the refractory state into account, the normalization condition writes: $\int_{-\infty}^{V_{th}} P(V,t)dV + \int_{t-\tau_r}^{t} r(s)ds$. The stationary firing rate for this model is shown in [98] to check:

$$r^{-1} = \sqrt{\pi} \int_{\frac{V_r-\mu}{\sigma}}^{\frac{V_r-\mu}{\sigma}} e^{s^2}(1+\mathrm{erf}(s))ds$$

with erf the error function

$$\mathrm{erf}(x) = \frac{1}{\pi}\int_{-x}^{x} e^{-s^2}ds.$$

2.7.4 Non-linear integrate and fire model.

The leaky integrate and fire neuron model is simple to use but has limited behavior and several more recent models have integrated a non-linearity to simulate the spiking mechanism and a secondary variable to provide an adaptation mechanism. This non-linearity is quadratic in the Izhikevich model [99] and exponential in the Brette-Gerstner model [100] and with such sophistications, the diversity observed in neuronal dynamics can be reproduced easily. The Brette-Gerstner model is driven by the following equation:

$$C\frac{dV}{dt} = -g_L(V-E_L) + g_L\Delta_T e^{\frac{V-V_T}{\Delta_T}} - w + I$$

$$\tau_w \frac{dw}{dt} = a(V-E_L) - w$$

with C, g_L and E_L the same parameters as in the LIF, Δ_T shaping the spike, I the external input, τ_m, the adaptation time scale and a scaling the contribution of the voltage to the adaptive variable dynamics. When $V > V_T$, the exponential term grows very fast corresponding to a spike and when the voltage crosses V_{cut}, the voltage is reset and the adaptation variable is increased:

$$\text{if } V > V_{cut} \left\{ \begin{array}{l} V = V_r \\ w = w + b \end{array} \right.$$

When $I < I_{th}$, the system set in a quiescent fixed point and $I > I_{th}$ leads to persistent firing of the neuron through saddle-node bifurcation if $a < \frac{g_L}{\tau_w}$ and through Andronov-Hopf bifurcation if $a > \frac{g_L}{\tau_w}$. The bifurcation to persistent firing when $a = \frac{g_L}{\tau_w}$ corresponds to a codimension two Bogdanov-Takens bifurcation [101].

2.7.5 Parameters for excitatory and inhibitory neurons.

Inhibitory neurons are usually considered to be fast spiking cells, with no adaptation, and excitatory neurons shows adaptive behavior with their firing rate slowly decreasing when a constant input is injected. Parameters used in the

Parameters of the membrane potential		
Membrane time constant [ms]: $\tau_m = \frac{C}{g_L}$		20
Membrane capacity [nF]: C		0.2
Membrane resting potential [mV]: E_L		-60
Reset membrane potential [mV]: V_r		-60
Threshold membrane potential [mV]: V_T		-50
Cutting membrane potential [mV]: V_{cut}		20
Refractory period [ms]: τ_r		5
Parameters of the synapse		
Excitatory synapse time constant [ms]: τ_{synE}		2
Inhibitory synapse time constant [ms]: τ_{synI}		1
Excitatory synapse reversal potential [mV]: E_{syn_E}		0
Inhibitory synapse reversal potential [mV]: E_{syn_I}		-80
Parameters of the adaptation variable	**Regular spiking (E)**	**Fast spiking (I)**
Increment of the adaptation variable: b	0.04	0
Scaling of the membrane potential contribution to the adaptation dynamics: a	0.001	.1
Adaptation time constant [ms]: τ_w	120	50

Figure 2.15: Parameter used for excitatory and inhibitory cells in the adaptive exponential integrate and fire neuron model.

simulations are listed in fig 2.15. The parameters for the regular spiking cell are taken from the result of fitting procedure on Hodgkin-Huxley model [102] or real data [103]. The average firing rate of a neuron connected to a Poisson input spike train is plotted for various input frequencies in fig 2.16. The adaptation added to the excitatory neuron linearizes this frequency-response curve.

2.8 Columns.

As we saw in the introduction, columnar structure support the modular view of the brain. There are still some controversy about what is the definition of a column and its internal structure.

2.8.1 Definition.

Anatomical column. During cell migration, minicolumnar structures can be seen and will stay in such a packed form in the adult neocortex. These microcolumns have around $50\mu m$ diameter and contain from 80 to 100 neurons. It has been supposed from the 80's that it is a uniform structure across areas and species but more recent observations found inter-individual and inter-species variability in the size and density in neurons of these columns [78].

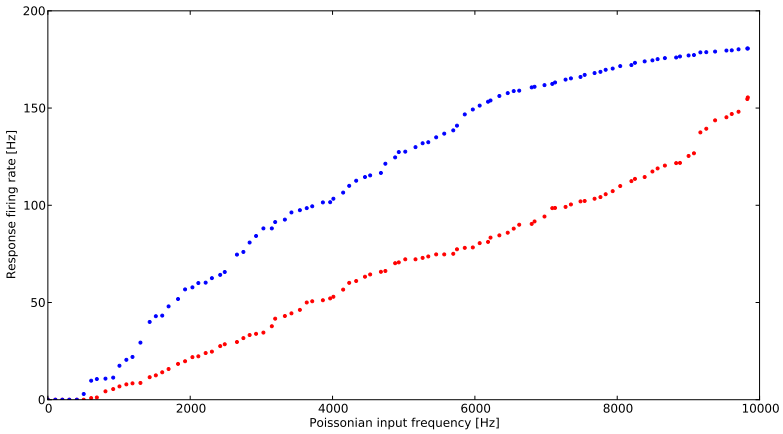

Figure 2.16: **Frequency-response curves.** - Average firing rate response to a Poisson input spike train at various frequencies for excitatory (red) and inhibitory (blue).

Functional column. At larger scale, as described in the introduction, functional columns are characterized by the response properties of its neurons. The diameter of a column is around $300\mu m$ and it is composed of around 60-80 minicolumns. Hypercolumns in primary visual cortex gathers cells having similar receptive field position but for which the preferred orientation may differ, it is around $1mm$ width. Columns related to more complex features can be found in inferotemporal cortex [104] or columns coding for a feature hold in memory can be found in prefrontal cortex [10].

2.8.2 Internal structure.

E-I network. The most common way to model a column is to consider a group of excitatory cells and a group of inhibitory cells. It is common to take 80% of excitatory cells and 20% of inhibitory cells. Composition of the network should also take the cell properties into account, with excitatory cells showing adaptation whereas inhibitory cells have fast spiking dynamics.

Neural circuit. A cortical column spans over 6 layers and networks accounting for this laminar structure are called neural circuits. In the Jansen and Rit model [105], three populations are considered for a column: one of excitatory pyramidal cells (located in layer II/III or layer V), one of inhibitory interneurons and one of excitatory interneurons located in IV. The LAMINART architecture also include three layers: II/III, IV and VI [106]. Detailed realizations of a neocortical column of the rat have also been realized including the detailed anatomy of the neuron in the blue brain project [80]. Templates based on the anatomical

studies of V_1 assessed the precise connection probabilities among the different layers and may offer a good description of the column (see [27] using data from [107] and [108]). More recent data describing a circuits of the visual cortex are available in [109].

2.9 Mean field equations.

Derivation of the Wilson-Cowan equations For a single column model, the activity is described by a macroscopic variable $x(t)$ describing the proportion of neurons firing at time t. After a neuron spikes, there is a refractory period τ_r during which the neuron is non responsive and for excitatory neurons, the proportion of neurons which are not in their refractory period at time t is

$$1 - \int_{t-\tau_r}^{t} X(t')dt'.$$

Neurons heterogeneity, introduced by a distribution $D(\theta)$ of firing threshold or a distrbution $C(w)$ on the number of afferent synapses to a neuron, shapes the response function, $S(x) = \int_0^x D(\theta)d\theta$ or $S(x) = \int_{\frac{\theta}{x}}^{\infty} C(w)dw$. This response can be taken as the sigmoid function, $S(x) = \frac{1}{1+e^{-a(x-\theta)}}$ whith the gain a and the threshold θ.

For a column with a level of recurrence α receiving the input β, the average excitation:

$$\int_{-\infty}^{t} h(t-t')(\alpha X(t') + \beta)dt'$$

with h an exponentially decreasing function. The dynamics then follow:

$$X(t+\tau) = (1 - \int_{t-\tau}^{t} X(t')dt')S(\int_{-\infty}^{t} h(t-t')(\alpha X(t') + \beta)dt'$$

By considering averages :$\bar{f}(t) = \frac{1}{s}\int_{t-s}^{t} f(t')dt'$, integrals can be approximated so that:

$$\int_{t-\tau}^{t} X(t')dt' \to r\bar{X}(t)$$

$$\int_{-\infty}^{t} h(t-t')X(t')dt' \to k\bar{X}(t)$$

By keeping X instead of $\bar{X}$ and using the Taylor formula $X(t+\tau) = X(t) + \tau\frac{dX}{dt} + o(\tau)$, we reach the following equation:

$$\tau\frac{dX}{dt} = -X + (1 - rX)S(\alpha X + \beta).$$

Bifurcations in a one excitatory population model Thus for a one population model with self-connection α and external input β, considering $r = 0$, the dynamics follows:

$$\frac{dx}{dt} = -x + S(\alpha x + \beta)$$

for which fixed points checks: $x_0 = S(\alpha x_0 + \beta)$. As shown on fig 2.17, there can be one or three fixed points depending on the parameters α, β. As the input β is varied, for sufficiently high values of the recurrence α, two saddle-nodde bifurcations occur when the linear part cancel out: $\alpha S'(\alpha x_0 + \beta) = 1$ which corresponds to the first diagonal $y = \frac{x}{\alpha}$ being tangent to the response function. As α is decreased, there is an α_c where the two saddle-node curves collide, this is the cusp of the system.

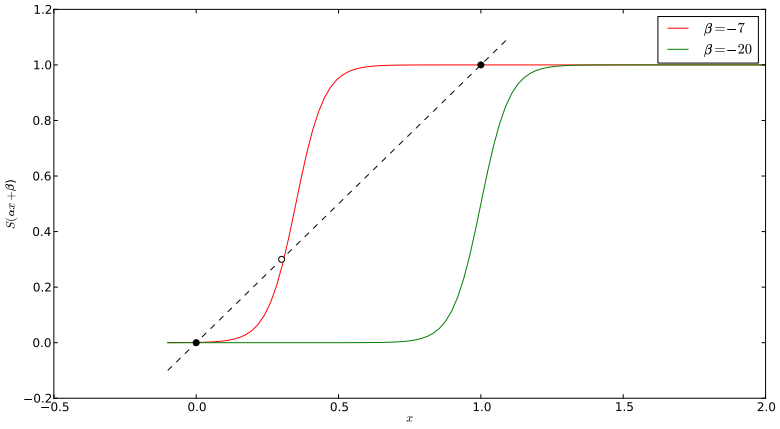

Figure 2.17: **Response function for various** β - There can be one or three fixed points depending on the number of intersection points between the response function and the line $g(x) = x$).

Phenomenological model of UP and DOWN states. Based on the previous demonstration of cusp bifurcation, the system can be approximated by its normal form near the bifurcation point. Near a cusp point, the population is described by the following dynamics: $\dot{x} = -\nabla E(r)$ deriving from the potential $E(r) = r^4 + ar^2 + bx$. When a goes from negative to positive values, the simple well potential becomes a double well potential and a scales the separation between the two fixed points and the height of the unstable fixed point. When the parameter $b = 0$, the double well potential is symmetric and one of the two fixed points has minimal potential when $b \neq 0$. The equation for the mean activity in a column is then:

$$dr = -(r^3 + ar + b)dt + \sigma dW_t.$$

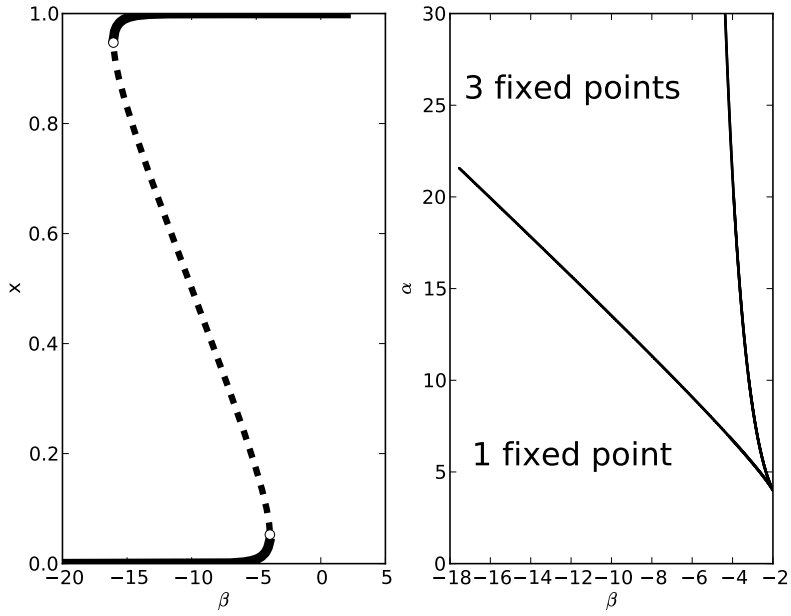

Figure 2.18: **Saddle-node bifurcation.** - (Left) SN bifurcations as β varies. (Right) Cusp point in the α, β.

When $a > 0$, the potential from which the dynamics derives has a single fixed point, $r_u = 0$, and the stochastic system has fluctuations around that fixed point whereas when $a < 0$, the corresponding potential has two fixed points, $r_s = \pm\sqrt{a}$, and transitions between these two fixed points are induced by noise. The corresponding Fokker-Planck equation is :

$$\frac{\partial p(r,t)}{\partial t} = \frac{\partial}{\partial r}(\nabla E(r) p(r,t)) + \frac{\sigma}{2}\frac{\partial^2 p(r,t)}{\partial r^2}$$

and the stationary distribution is:

$$p_0(r) = \mathcal{N} e^{\frac{-2\nabla E(r)}{\sigma}}.$$

The time between transition from one of the stable node to the other is given by the inverse of the Kramers rate [87]:

$$T_s = \frac{\pi}{|\sqrt{E''(r_u)|E''(r_s)}} e^{\frac{E(r_u)-E(r_s)}{\sigma}}.$$

If an additional low frequency, ω, forcing is added to the system, there is a noise intensity for which coherent transitions occurs between the two fixed points. The condition for such stochastic resonance is $2T_s = T_\omega$.

The description of the network activity in terms of attractors was used in a more sophisticated network modeling decision making in [110].

Bifurcations in the two populations model of a column. According to Dale's principle, neuronal cells should be considered based on their synaptic influence on other cells, into excitatory and inhibitory cells leading to the mean-field model:

$$\tau_e \frac{dE}{dt} = -E + (1 - r_e E) S(a_e(c_1 E - c_2 I - \theta_e + P))$$

$$\tau_i \frac{dI}{dt} = -I + (1 - r_i I) S(a_i(c_3 E - c_4 I - \theta_i + Q))$$

The system then have one or several fixed points or even limit cycles as shown in these classical results from Wilson and Cowan in [111]:

- If $c_1 > \frac{9}{a_e}$, there are some constant (P,Q) configurations for which the system has 3 fixed points.
- If $\frac{a_e c_2}{a_e c_1 - 9} > \frac{a_i c_4 + 9}{a_i c_3}$, there are some constant (P,Q) configurations for which the system has 5 fixed points.
- If $c_1 a_e > c_4 a_i + 18$, at least one fixed point is unstable.
- If $\frac{a_e c_2}{a_e c_1 - 9} > a_i c_4 + 9 a_i c_3$, $\frac{a_e c_1 - 9}{a_e c_2} < 1$ and the preceding condition for fixed point instability holds, then for $Q = 0$, there exists a threshold P_0 such by increasing P, a limit cycle appears when $P > P_0$.

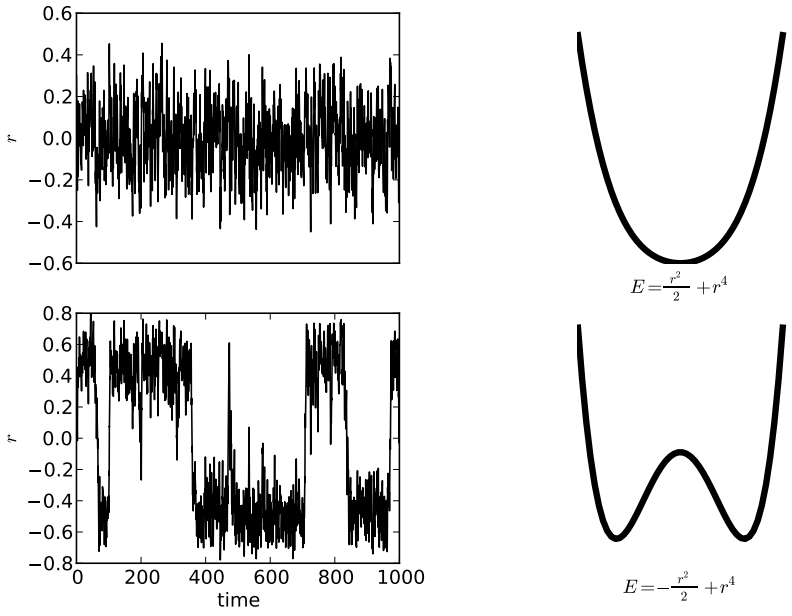

Figure 2.19: **Stochastic forcing of the normal form near the cusp bifurcation.** - (Up) $a > 0$, the firing rate r shows fluctuations around the single fixed point. (Down) $a < 0$, r has stochastic transitions between the two fixed points.

2.10 A column of spiking neurons.

The network is composed of two populations, 80% of the cells are excitatory and 20% are inhibitory. Excitatory cells are regular spiking with adaptation and inhibitory ones are fast spiking. When connections in the network are considered as sparse, there can be several behaviors depending on the balance between excitation and inhibition. For high values of the maximal excitatory conductance with low value of the inhibitory conductance, the network saturates to its maximal frequency and for higher values of the maximal inhibitory conductance, the network have collective oscillations or asynchronous state. The asynchronous irregular regime was first described in a theoretical work of Van Vreeswijk and Sompolinsky in [33] for a network of sparsely connected binary neurons with excitatory currents balancing precisely the inhibitory ones and this asynchronous state was later reported for integrate and fire neurons with current synapses [112] or conductance synapses [113].

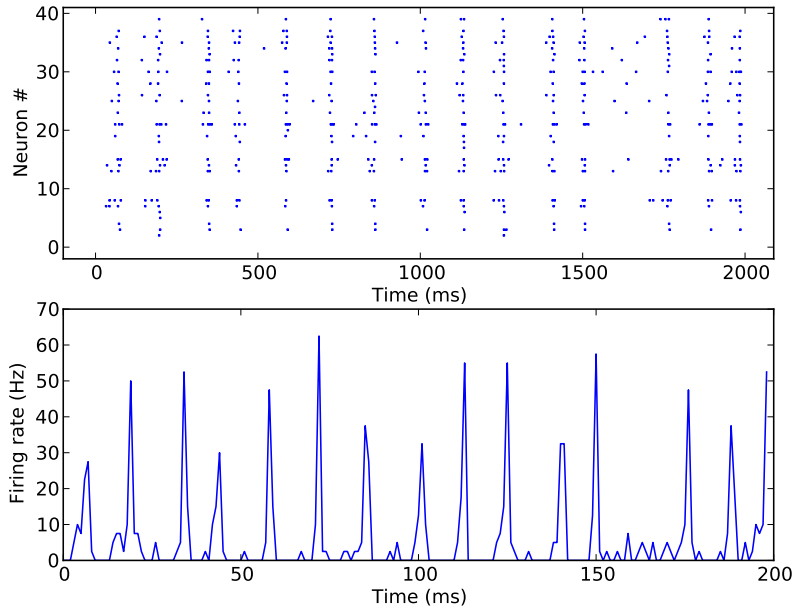

Figure 2.20: **Activity of the 40 excitatory neurons in a column composed of 50 neurons.** - (Up) Raster plot of a column. (Down) Average firing rate in the column.

Asynchronous irregular regime in a network of binary neurons. The network is composed of two populations, one with N_E excitatory neurons and

one with N_I inhibitory neurons. At each time, a neuron i from population k gets its state updated according to: $\sigma_i^k(t) = H(u_i^k(t))$ where H is the Heaviside function $H(x) = \begin{cases} 0 & \text{if } x < 0 \\ 1 & \text{if } x \geq 0 \end{cases}$ and $u_i^k(t)$ is the input to the neuron i at time t:

$$u_i^k(t) = \sum_{l=E,I} \sum_{j=1}^{N_k} J_{ij}^{lk} \sigma_j^l(t) + u_0^k - \theta_k$$

with u_0^k the external input and θ_k the threshold for neurons of the population k. Each neuron receive input from K neurons with connection strength $J_{ij}^{kl} = \frac{J_{kl}}{\sqrt{K}}$ so that the network is sparsely connected: $1 << K << N$. Moreover, because the absolute scale of the input is of no relevance, it is possible to consider $J_{EE} = J_{EI} = 1$ and $J_E = -J_{IE}$, $J_I = -J_{II}$. The population averaged firing rate is $m_k = \frac{1}{N_k} \sum_{i=1}^{N_k} \sigma_i^k(t)$ and it checks the mean field equation [33]:

$$\tau_k \frac{dm_k(t)}{dt} = -m_k(t) + \text{erf}(-\frac{u_k}{\alpha_k})$$

with the mean input for neurons of the population k:

$$u_k(t) = \sqrt{K}(\sum_{l=E,I} J_{lk} m_l(t) + E_k m_0) - \theta_k$$

where m_0 is the mean rate of external sources connecting with strength $\frac{E}{\sqrt{K}}$ to the excitatory population and $\frac{I}{\sqrt{K}}$ to the inhibitory population, and the variance of the input to the population is

$$\alpha_k(t) = \sum_{l=1,2} (J_{lk})^2 m_l(t).$$

The complementary error function is:

$$erf(z) = \int_z^\infty e^{-\frac{x^2}{2}} \frac{dx}{2\pi}.$$

Apart from saturating fixed points resulting in $m_E, m_I = 0, 1$ or $m_E, m_I = 1, 0$, there can be a balanced fixed with finite inputs so that:

$$Em_0 + m_E - J_E m_I = \text{O}(\frac{1}{\sqrt{K}})$$

$$Em_0 + m_E - J_I m_I = \text{O}(\frac{1}{\sqrt{K}})$$

so that as $K \to \infty$:

$$m_E = \frac{J_I E - J_E I}{J_E - J_I} m_0$$

$$m_I = \frac{E - I}{J_E - J_I} m_0$$

and the balanced state can exist if these stationary firing rates are positive, that is if:

$$\frac{E}{I} > \frac{J_E}{J_I} > 1$$

or

$$\frac{E}{I} < \frac{J_E}{J_I} < 1.$$

Furthermore there can be unbalanced solution $m_E, m_I = 1, 1$ with inputs $u_k = \sqrt{K}$ of order $\sqrt{K}$ if

$$\frac{E}{I} < \frac{J_E}{J_I} < 1$$

or if $1 > J_E$ and $1 > J_I$ so that the conditions to obtain a balanced state are:

$$\frac{E}{I} > \frac{J_E}{J_I} > 1$$

and

$$J_E > 1.$$

The balanced state achieve perfect tracking of a time varying input with the effective time constant being much smaller than for the unbalanced state.

Fokker-Planck equations for a column of integrate-and-fire neurons. A network with a similar column architecture was studied with integrate-and-fire neurons as units of the network [112]. The dynamics for each neuron is:

$$\frac{dV_i}{dt} = -\frac{1}{\tau}V_i + \sum_j \sum_k J_{ij}\delta(t - t_k - D)$$

and if

$$V_i(t) > V_{th}, V_i(t + \tau_{ref}) = V_r$$

where k runs over spikes of the neuron j and j runs over the input neurons to the neuron i consisting of C_{ext} neurons from the external source, $C_E = \epsilon N_E$ neurons from the excitatory population and $C_I = \epsilon N_I$ neurons from the inhibitory population with $\epsilon << 1$ so that connections are sparse. Moreover, notations are simplified by taking $C_I = \gamma C_E$. The delay D stands for the propagation time along the axon and the dendritic tree. The PSP amplitude for external and recurrent synapses are taken to be equal, J, and for the inhibitory synapses, the PSP amplitude is gJ. For such a network, the Langevin equation is:

$$\tau\frac{dV_i}{dt} = -V_i + \mu(t) + \sigma\sqrt{\tau}\eta_i(t)$$

with the average and variance of the input composed of a recurrent part and an external part, both resulting from Poissonian spike trains :

$$\mu(t) = C_E J(1 - \gamma g)\nu(t - D)\tau + C_E J\nu_{ext}\tau$$

and

$$\sigma = J\sqrt{C_E(1+\gamma g)\nu(t-D)\tau + C_E\nu_{ext}}.$$

The corresponding Fokker Planck equation for the probability density of the membrane voltage is

$$\frac{\partial P(v,t)}{\partial t} = \frac{\partial}{\partial V}((V-\mu(t))P(V,t)) + \frac{\sigma^2}{2}\frac{\partial^2 P(V,t)}{\partial V^2}$$

which can be rewritten in terms of probability flux:

$$\frac{\partial P(V,t)}{\partial t} = -\frac{\partial S(V,t)}{\partial V}$$

with

$$S(V,t) = -(V-\mu(t))P(V,t) - \frac{\sigma^2}{2}\frac{\partial P(V,t)}{\partial V}.$$

Boundary conditions should be precised for this equation to have a unique solution.

- At the threshold voltage, the probability flux gives the firing rate and this firing rate stays finite so that $S(V_{th},t) = \nu(t)$ and $P(V,t) = 0$ for $V \geq V_{th}$. This results in $\frac{\partial P(V_{th},t)}{\partial V} = -\frac{2\nu(t)\tau}{\sigma^2(t)}$.
- At the reset potential, the probability distribution is continuous and the probability flux from the threshold potential is reinjected taking the refractory period into account so that the probability flux has the following discontinuity $S(V_r^+,t) - S(V_r^-,t) = \nu(t-\tau_{ref})$ or

$$\frac{\partial P(V_r^+,t)}{\partial V} - \frac{\partial P(V_r^-,t)}{\partial V} = -\frac{2\nu(t-\tau_{ref})\tau}{\sigma^2(t)}.$$

- The integral of the probability distribution should stay finite so that $P(V,t) \to 0$ and $VP(V,t) \to 0$ when $V \to -\infty$.
- Finally, as a probability distribution, it checks the following normalization condition:

$$\int_{-infty}^{V_{th}} P(V,t)dV + \int_{t-\tau_{ref}}^{t} \nu(u)du = 1.$$

The stationary distribution solution of the Fokker Planck equation with such conditions for the voltage is

$$P_0(V) = \frac{2\nu_0\tau}{\sigma_0} e^{-\frac{(V-\mu_0)^2}{\sigma_0^2}} \int_{\frac{V-\mu_0}{\sigma_0}}^{\frac{V_{th}-\mu_0}{\sigma_0}} H(u-V_r)e^{u^2}du$$

. With H the Heaviside function, $H(x) = 1$ if $x > 0$ and $H(x) = 0$ otherwise, and

$$\mu_0 = C_E J\tau(\nu_{ext} + \nu_0(1-g\gamma)$$

$$\sigma_0^2 = C_E J^2 \tau(\nu_{ext} + \nu_0(1 + g^2\gamma)).$$

The normalization condition gives the stationary firing rate ν_0:

$$\frac{1}{\nu_0} = \tau_{ref} + 2\tau \int_{\frac{V_r-\mu_0}{\sigma_0}}^{\frac{V_{th}-\mu_0}{\sigma_0}} du e^{u^2} \int_{-\infty}^{u} dv e^{-v^2}.$$

Linear stability analysis gives the Hopf bifurcation lines where transition to synchronous spiking occurrs. The computation of the coefficient of variation of interspikes intervals on numerical simulations of the network then determines whether the spiking is regular or irregular. The diagram for the network with uniform delays $D = 1.5ms$ is shown on fig 2.21 depending on the external frequency and the relative strength of excitatory and inhibitory currents. There are three lines separating asynchronous behaviour from synchronous instabilities:

- A vertical line at $g = 4$ corresponds to exact balancing of inhibitory and excitatory currents. For $g < 4$, the activity is synchronous regular at high frequency and for $g > 4$, neurons spike at low frequency asynchronously.
- For $g > 4$, at low external input frequency, a branch separates the asynchronous irregular state from a low frequency synchronous irregular regime.
- For $g > 4$, at high external input frequency, a branch separates the asynchronous irregular state from a high frequency synchronous irregular regime.

Moreover, in the triangular region near $g = 4$ and with external frequency close to threshold, the activity combines a slow oscillation and a high frequency spiking on top of it.

2.11 Coupled columns.

2.11.1 Reduction to oscillators.

For two weakly coupled columns, the mean field equations are:

$$\begin{cases} \frac{dE_k}{dt} &= -E_k + S(A_k^e + \eta a_e U_l) \\ \frac{dI_k}{dt} &= -I_k + S(A_k^i + \eta a_i V_l) \end{cases}$$

with populations $k, l = 1, 2$ $k \neq l$ and

$$U_l = a_1 E_1 - a_2 I_l$$

$$V_l = a_3 E_l - a_4 I_l$$

$$A_k^e = a_e(c_1 E_k - c_2 I_k - \theta^e + P_k)$$

$$A_k^i = a_e(c_3 E_k - c_4 I_k - \theta^i).$$

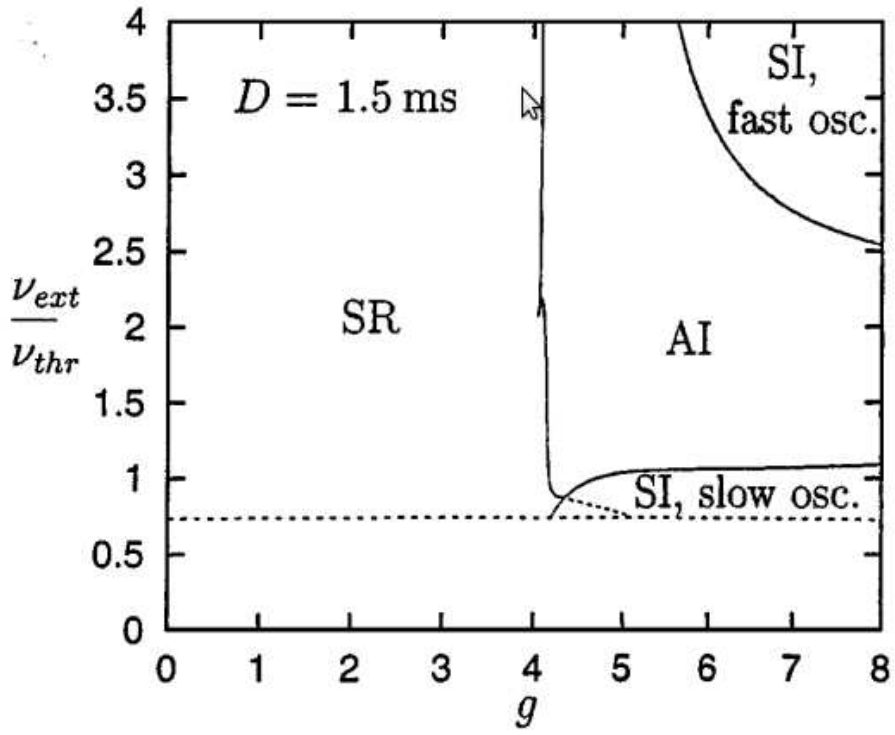

Figure 2.21: **Diagram of a network of IF neurons (Adapted from [112]).** - Parameters are the relative strength of inhibition g and the frequency of the external input rescaled by the frequency needed to reach threshold without feedback, $\nu_{th} = \frac{V_{th}}{C_E J \tau}$. Possible states are described as asynchronous (A), synchronous (S), regular (R) or irregular (I).

A change of variables leads to the Hopf normal form and the reduction of the oscillators to their phases ϕ_1, ϕ_2 leads to the system:

$$\begin{cases} \frac{d\phi_1}{dt} &= \omega_1 - K_{12} sin(\phi_1 - \phi_2) \\ \frac{d\phi_2}{dt} &= \omega_2 - K_{21} sin(\phi_2 - \phi_1) \end{cases}$$

with coupling terms proportional to $\eta a_e S'(A^e_k)$ and $\eta a_e S'(A^i_k)$.

2.11.2 Few coupled columns.

Arnold tongues. For a single oscillator with forcing frequency ω and self-coupling K:

$$\frac{d\phi}{dt} = \omega - K sin(\phi)$$

various mode locking are possible depending on ω and K. Arnold tongues are regions of the parameter space where the mode locking index $\frac{\dot{\phi}}{\omega}$ is uniform. The largest areas are integer modes and smaller areas are fractional modes, modes $0, \frac{1}{2}, 1, \frac{3}{2}, 2$ can be seen on fig 2.22.

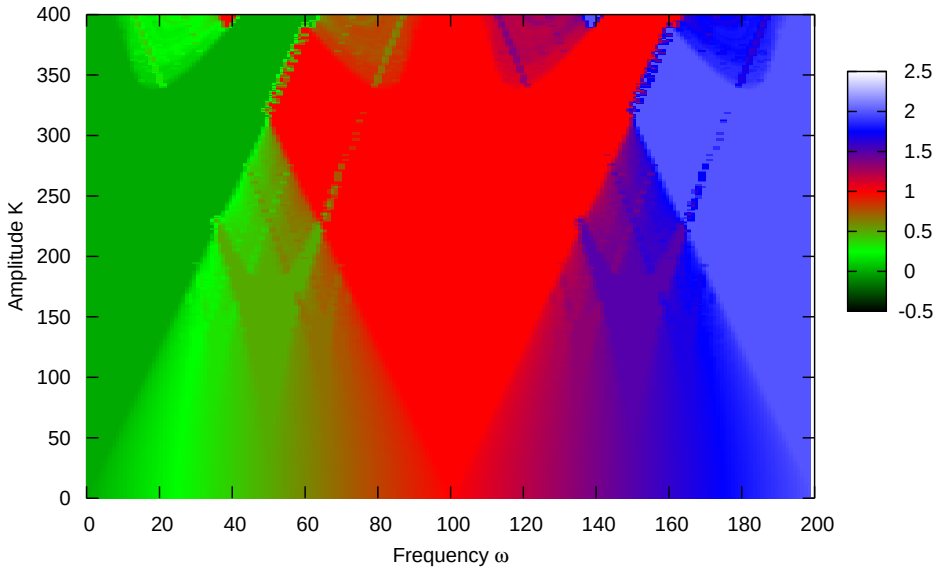

Figure 2.22: **Arnold tongues.** - Mode locking index $\frac{\dot{\phi}}{\omega}$ depending on the intrinsic frequency ω and the self-coupling K.

Synchronization transition. For two coupled oscillators forced at frequencies ω_1 and ω_2 and symmetrically coupled with strength K, it is convenient to consider the phase difference $\psi = \phi_1(t) - \phi_2(t)$ which follows:

$$\frac{d\psi(t)}{dt} = \Delta\omega + 2K\sin\psi$$

with $\Delta\omega = \omega_1 - \omega_2$. If the coupling is strong enough, the stationary phase difference is $\Delta\phi = \arcsin\frac{-\Delta\omega}{2K}$. If $K < K_c = \frac{\Delta\omega}{2}$, there is no stationary solution. There is thus a frequency synchronization transition at K_c and it is a second order transition as the order parameter is continuous and its derivative is discontinuous at the transition point. The transition can be seen on fig 2.23 where the average phase difference, $\Delta\phi = \frac{1}{T}\int_0^T \psi dt$, is plotted as a function of the coupling strength for oscillators frequencies, $\omega_1 = 1.2$ and $\omega_2 = 1$.

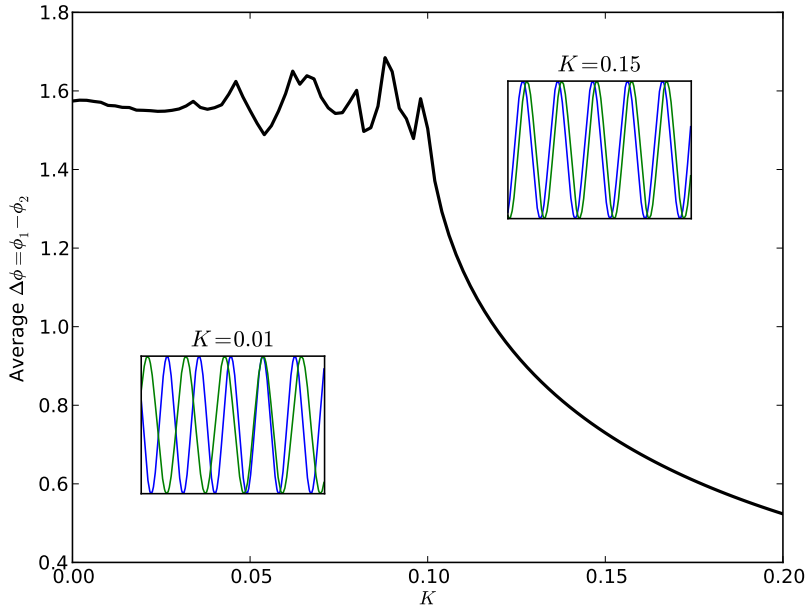

Figure 2.23: **Synchronization of two oscilators depending on the coupling K.** - The average phase difference is constant until K_c at which the two oscillators start getting synchronized.

Partial synchronization. With three oscillators, partial synchronization occurs as the coupling strength K is increased with oscillators with closest frequency synchronizing first. The sequence of such synchronization transitions is shown for three oscillators of frequencies $\omega_1 = 1$, $\omega_2 = 0.4$ and $\omega_3 = 0.2$ in fig

2.24 where the instantaneous frequencies of oscillators are plotted as a function of the coupling strength K.

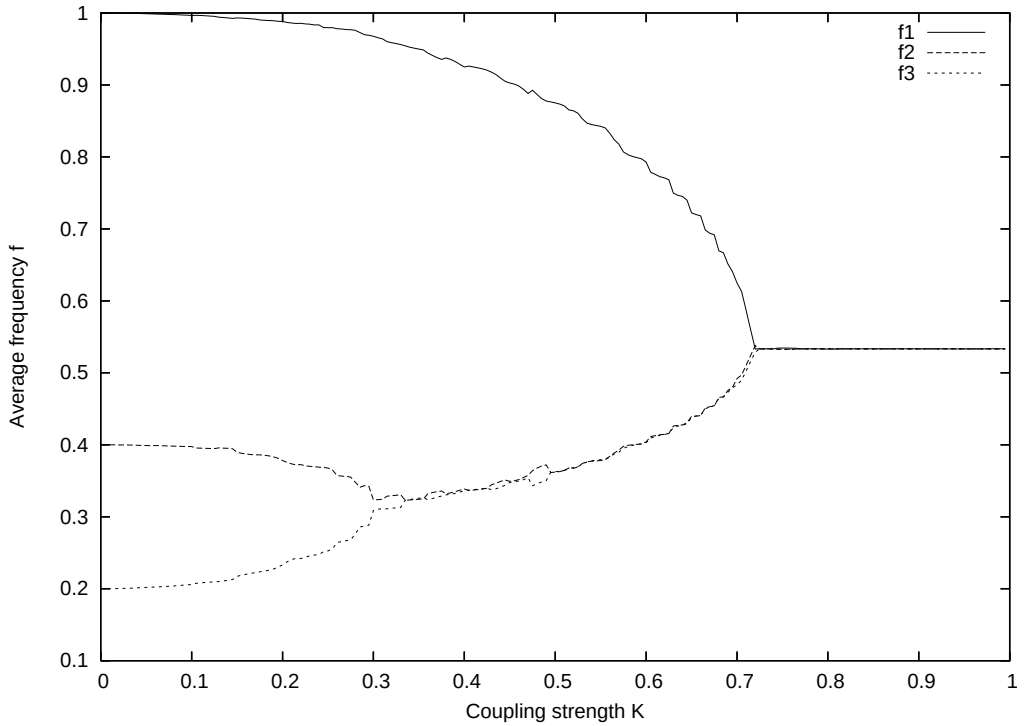

Figure 2.24: **Partial synchronization for 3 oscillators.** - For loose coupling, oscillators run at their intrinsic frequency, for intermediate values of the coupling only the two oscillators with the closest frequency are frequency locked and for higher values of the coupling, the network oscillates in full synchrony.

For $N \geq 4$, phase chaos was shown to occur through torus destruction as the coupling strength is increased [114].

2.11.3 Large population of coupled oscillators.

A population of globally coupled oscillators. The Kuramoto model is widely used to study synchronization between coupled units [115] and it is composed of N oscillators coupled, with $N >> 1$, according to the equations:

$$\frac{d\phi_i}{dt} = \omega_i + \sum_j K_{ij} sin(\phi_j - \phi_i)$$

with $1 \leq i \leq N$, intrinsic frequencies distributed according to $g(\omega)$ and the original model the coupling is homogeneous $K_{ij} = \frac{K}{N} > 0$. The dynamics can

then be written as:

$$\frac{d\phi_i}{dt} = \omega_i + Krsin(\psi - \phi_i)$$

with the order parameter defined as $re^{i\psi} = \frac{1}{N}\sum_k e^{i\phi_k}$, $r \in [0,1]$ measures the coherence in the population and ψ is the average phase. The coherence is $r = 0$ for weak coupling with oscillators moving independently and it is $r = 1$ when strong coupling makes all phases equal to ψ. Equivalently, the order parameter can be expressed a function of the probability distributions for intrinsic frequencies ,$g(\omega)$, and for the phases, $\rho(\phi, \omega, t)$:

$$re^{i\psi} = \int_{-\pi}^{\pi}\int_{-\infty}^{\infty} e^{i\phi}\rho(\phi,\omega,t)d\omega d\phi.$$

Moreover, the distribution ρ satisfies the continuity equation:

$$\frac{\partial\rho}{\partial t} + \frac{\partial}{\partial\phi}[(\omega + rsin(\psi - \phi)\rho]$$

and the normalization condition:

$$\int_{-\pi}^{\pi}\rho(\omega,\phi,t)d\phi.$$

The incoherent solution corresponds to $r = 0$ and $\rho = \frac{1}{2\pi}$ with all phases having equal probability of being occupied. A branch of partially synchronized solutions starts at $K_c = \frac{2}{\pi g(0)}$ and with a Loretzian distribution [9] for g, the coherence behaves as $r = \sqrt{1 - \frac{K_c}{K}}$.

Chimera states. We now consider a ring of oscillators with long range connections:

$$\frac{d\phi(x,t)}{dt} = \omega + \int_0^1 K(x,x')sin(\phi(x,t) - \phi(x',t) + \alpha)dx'$$

where the connections are made through a Gaussian kernel $K(x,x') = Ae^{-\frac{|x-x'|^2}{2\sigma^2}}$. With initial condition constant over an interval and randomly distributed with a Gaussian profile on its complementary, the network settle in a chimera state where a part of the network is phase locked and the other part is oscillating in an asynchronous manner as shown in fig 2.25.

Flip-flop network. A network of oscillators can be coupled to Wilson-Cowan units with equations:

$$\frac{dx_i}{dt} = -x_i + \sigma(cos(\phi) - cos(\phi_0)) + \sum_j w_{ij}f(x_j) + I$$

[9] A Lorentzian distribution is of the form $g(\omega) = \frac{\gamma/\pi}{\gamma^2+\omega^2}$.

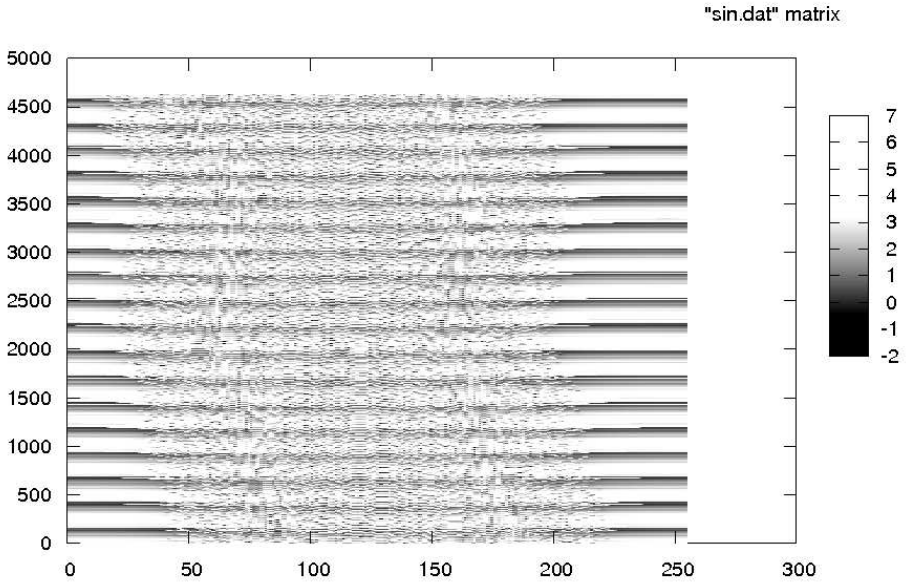

Figure 2.25: **Chimera state.** - Ring of oscillators with a part of the network phase locked and the complementary oscillating asynchronously.

$$\frac{d\phi_i}{dt} = \omega + (\beta - \rho x_i) sin(\phi_i)$$

where x_i is the membrane voltage of the component i and $cos(\phi_i)$ is an oscillating contribution to the dynamics scaled by σ and the membrane impacts the oscillators dynamics by a factor rho. $f(x_i)$ is the firing rate of the neuron i taken as an hyperbolic tangent and ϕ_0 is chosen so that the state where $(x_i, \phi_i) = (0, \phi_0)$ is a fixed point for the network. The conditions for stability of this fixed point are given in [116] reproduced in appendix. Two coupled units show down state, low frequency, antiphase oscillation for weak coupling and up state, high frequency, in-phase oscillation for large coupling. Before the phase-locked solution exists, a small window of chaotic behaviour is observed. In a larger network, the spontaneous activity wanders around cell assemblies storing memories.

2.12 Conclusion.

In this chapter, we explored the dynamics of computational units of the brain using bifurcation theory and the Fokker-Planck equation. The Hodgkin Huxley model for the dynamics of the membrane potential of a neuron is difficult to analyze and heavy to integrate. The FitzHugh Nagumo model is a reduction of the dynamics to a two dimensional phase model controlled by three parameters. With the analysis of bifurcations in this system, we found an organizing center for the dynamics in the neighborhood of which any possible dynamics is accessible. Stochastic forcing at this point resulted in the emergence of multiple timescales which may be traces of the attractors available in its neighborhood: limit cycle for the fast timescale and stochastic transitions between two fixed points for the slow timescale. We also noticed, for identical realizations of the noise, that the formant of the dynamics increases in a plateau like fashion when increasing the variance of the noise. The integrate and fire model is another phenomenological model commonly used for efficient simulation and we introduced a two dimensional version, the adaptive integrate and fire neuron which have a large repertoire of dynamics. For a column, mean field models provides a compact description and the network activity can be characteried by the synchrony and the regularity of firing. When columns have a collective oscillation resulting from a Hopf bifurcation in their mean field equation, the rich variety of possible dynamics was described using networks of coupled phase oscillators: resonance, frequency synchrony, phase synchrony and chimera states.

We saw that the asynchronous state described in the first part can be modeled as the chaotic dynamics of a balanced network of sparsely connected binary neurons. Networks of spiking neurons have a similar state and it can even be self-sustained for a very long time with conductance based neurons. The length of these supertransients of irregular activity depends exponentially on the size of the network [34]. The computation of Lyapunov exponents for hybrid dynamical systems needs special care [117] and when the largest of these exponent is not positive, this state is called stable chaos. Chaotic behavior of a macroscopic

variable, collective chaos, and chimera states have also been reported recently in networks of spiking neurons [118]. Neuronal networks thus have rich variety of dynamics and their potential use for solving computational tasks offers new approaches in artificial intelligence [119].